Inorganic Chemistry
Forum Article

*Inorg. Chem.* **2010**, *49*, 6293–6316 **6293**
DOI: 10.1021/ic902304a

# Electronic Structure of Heme-Nitrosyls and Its Significance for Nitric Oxide Reactivity, Sensing, Transport, and Toxicity in Biological Systems

**Lauren E. Goodrich, Florian Paulat, V. K. K. Praneeth, and Nicolai Lehnert***

*Department of Chemistry, University of Michigan, Ann Arbor, Michigan 48109*

Received November 20, 2009

This review summarizes recent developments in the investigation of the electronic structures, spectroscopic properties, and reactivities of ferrous and ferric heme-nitrosyls and how this relates to important biological processes. Ferrous heme-nitrosyls show interesting variations in electronic structure as a function of the different types of proximal ligands, as is evident from electron paramagnetic resonance, magnetic circular dichroism, and vibrational spectroscopy. In particular, coordination of imidazoles like histidine (His) increases the radical character on NO and, in this way, could help activate the bound NO for catalysis. Vice versa, the bound NO ligand imposes a strong $\sigma$ *trans* effect on the proximal His, which, in the case of soluble guanylate cyclase (sGC), the biological NO sensor protein, induces breaking of the $Fe^{II}$—His bond and activates the protein. The possibility of sGC activation by HNO is also discussed. Finally, the properties of ferrous heme-nitrosyls with proximal cysteinate (Cys) coordination are evaluated. It has been known for some time that ferric heme-nitrosyls are intrinsically more labile than their ferrous counterparts, but the underlying reasons for this observation have not been clarified. New results show that this property relates to the presence of a low-lying excited state that is dissociative with respect to the $Fe^{III}$—NO bond. On the other hand, the ground state of these complexes is best described as $Fe^{II}$—$NO^{+}$, which shows a very strong Fe—NO bond, as is evident from vibrational spectroscopy. NO, therefore, is a weak ligand to ferric heme, which, at the same time, forms a strong Fe—NO bond. This is possible because the thermodynamic weakness and spectroscopic strength of the Fe—NO bond relate to the properties of different electronic states. Thiolate coordination to ferric hemes leads to a weakening of both the Fe—NO and N—O bonds as a function of the thiolate donor strength. This observation can be explained by a $\sigma$ backbond into the $\sigma^*$ orbital of the Fe—N—O unit that is mediated by the thiolate $\sigma$-donor orbital via orbital mixing. This is a new interaction in heme-nitrosyl that has not been observed before. This also induces a bending of the Fe—N—O subunit in these cases. New spectroscopic data on a corresponding model complex are included in this paper. Finally, the mechanism of NO reduction by cytochrome P450nor is elucidated based on recent density functional theory results.

## A. Introduction

Historically, nitric oxide (nitrogen monoxide, NO) has always been viewed as an environmental pollutant, generated from the burning of fossil fuels, because of its toxic and corrosive properties. Together with its homologue nitrogen dioxide ($NO_2$), it is one of the main contributors to smog. NO is poisonous to humans at very low concentrations of only 100 ppm in air. This dose is rated as immediately dangerous to life or health by the National Institute for Occupational Safety and Health. The general view of NO as an environmental pollutant and toxin changed dramatically in the 1980s when it was first realized that humans are capable of NO biosynthesis for the purpose of immune defense and signaling.[1−7] In 1992, NO was therefore voted the molecule of the year by the magazine *Science*,[8] followed by the Nobel Prize in Medicine in 1998.

**NO Biosynthesis.** In mammals, NO is generated by nitric oxide synthase (NOS) isozymes, which belong to the cytochrome P450 family.[9−14] For the purpose of

*To whom correspondence should be addressed. E-mail: lehnertn@umich.edu.

(1) Moncada, S.; Palmer, R. M.; Higgs, E. A. *Pharmacol. Rev.* **1991**, *43*, 109–142.
(2) Snyder, S. H. *Science* **1992**, *257*, 494–496.
(3) Butler, A. R.; Williams, D. L. H. *Chem. Soc. Rev.* **1993**, 233–241.
(4) Bredt, D. S.; Snyder, S. H. *Annu. Rev. Biochem.* **1994**, *63*, 175–195.
(5) Lancaster, J. R., Jr. In *Encyclopedia of Inorganic Chemistry*; Bruce, R. B., Ed.; Wiley: Chichester, U.K., 1994.
(6) Feelisch, M.; Stamler, J. S. *Methods in Nitric Oxide Research*; Wiley: Chichester, U.K., 1996.
(7) Ignarro, L. *Nitric Oxide: Biology and Pathobiology*; Academic Press: San Diego, 2000.
(8) Culotta, E.; Koshland, D. E., Jr. *Science* **1992**, *258*, 1862–1865.
(9) Stuehr, D. J. *Annu. Rev. Pharmacol. Toxicol.* **1997**, *37*, 339–359.
(10) Raman, C. S.; Li, H.; Martasek, P.; Kral, V.; Masters, B. S. S.; Poulos, T. L. *Cell* **1998**, *95*, 939–950.
(11) Fischmann, T. O.; Hruza, A.; Niu, X. D.; Fossetta, J. D.; Lunn, C. A.; Dolphin, E.; Prongay, A. J.; Reichert, P.; Lundell, D. J.; Narula, S. K.; Weber, P. C. *Nat. Struct. Biol.* **1999**, *6*, 233–242.
(12) Li, H.; Poulos, T. *J. Inorg. Biochem.* **2005**, *99*, 293–305.
(13) Rousseau, D. L.; Li, D.; Couture, M.; Yeh, S.-R. *J. Inorg. Biochem.* **2005**, *99*, 306–323.


Published on Web 07/12/2010

signaling, NO is produced by endothelial (e-) NOS in the endothelial cells that line the inner surface of arteries (blood pressure control) or by neuronal (n-) NOS in the brain for nerve signal transduction.[15] NO is also produced in macrophages by inducible (i-) NOS for immune defense.[16−20] NO is very effective in this respect: for example, exposure of cultures of *Mycobacterium tuberculosis* to $< 100$ ppm of NO killed $> 99\%$ of the bacteria in the culture.[21] In all cases, the biosynthesis of NO starts from L-arginine, which is first hydroxylated and then oxidized to yield citrulline and NO.[22−28]

In denitrifying bacteria or fungi, NO is produced by copper- or iron-containing nitrite reductases (NIRs).[29] Denitrifying organisms live in soil and seawater under anaerobic conditions and use the stepwise reduction of nitrate to $N_2$ for anaerobic respiration.[30−32] The iron enzyme, referred to as heme $cd_1$ NIR, contains a heme *c* and a heme $d_1$ per subunit, the latter being the catalytically active site.[29] In the reduced, ferrous oxidation state, five-coordinate (5C) heme $d_1$ binds nitrite, supposedly via its N atom,[33−38] followed by reduction and dehydration of this ligand, yielding water and a ferric heme $d_1$ nitrosyl as the enzyme−product complex. A loss of NO and electron transfer from heme *c* completes the catalytic cycle. A corresponding NIR reaction has also been invoked for the generation of NO upon curing of meat, i.e., by the reaction of nitrite with deoxy-Hb and -Mb.[39−41] This reaction has gained significant attention recently as a means to generate NO *in vivo* in the process of hypoxic vasodilation.[42,43] Since nitrite is present in plasma (50−500 nM) and tissues (0.5−25 $\mu$M), it is readily available to react with deoxygenated Hb to form NO and ferric met-Hb,[44−46] which could then bind additional nitrite and react with NO to generate $N_2O_3$ as an NO carrier and nitrosylating agent.[47] In this way, blood flow could be directed to hypoxic tissue. This process might also be involved in the production of S-nitrosylated Hb (SNO-Hb), which, by itself, is invoked as an alternative mediator for hypoxia sensing.[48−51]

**Biological NO Sensing.** The important cardiovascular regulation (vasodilation) by NO (produced by e-NOS)[52,53] is then mediated by soluble guanylate cyclase (sGC).[54−60] This enzyme serves as the general biological NO sensor/receptor in mammals. In its active form, sGC contains a 5C heme with proximal histidine (His) coordination in the ferrous oxidation state. Upon binding of NO, a six-coordinate (6C) ferrous heme-nitrosyl is believed to form as an intermediate. Because of the strong *σ trans* interaction between NO and the axial His ligand,[61−68] the $Fe^{II}$−His bond is broken, leading to the corresponding 5C ferrous heme NO complex. This is

(14) Martin, N. I.; Woodward, J. J.; Winter, M. B.; Beeson, W. T.; Marletta, M. A. *J. Am. Chem. Soc.* **2007**, *129*, 12563–12570.
(15) Montague, P. R.; Gancayco, C. D.; Winn, M. J.; Marchase, R. B.; Friedlander, M. J. *Science* **1994**, *263*, 973–977.
(16) Stuehr, D. J.; Gross, S. S.; Sakuma, I.; Levi, R.; Nathan, C. F. *J. Exp. Med.* **1989**, *169*, 1011–1020.
(17) MacMicking, J.; Xie, Q.-W.; Nathan, C. *Annu. Rev. Immunol.* **1997**, *15*, 323–350.
(18) Drapier, J.-C.; Pellat, C.; Henry, J. *J. Biol. Chem.* **1991**, *266*, 10162–10167.
(19) Stadler, J.; Bergonia, H. A.; Di Silvio, M.; Sweetland, M. A.; Billiar, T. R.; Simmons, R.; Lancaster, J. R. *Arch. Biochem. Biophys.* **1993**, *302*, 4–11.
(20) Terenzi, F.; Diaz-Guerra, J. M.; Casado, M.; Hortelano, S.; Leoni, S.; Boscá, L. *J. Biol. Chem.* **1995**, *270*, 6017–6021.
(21) Long, R.; Light, B.; Talbot, J. A. *Antimicrob. Agents Chemother.* **1999**, *43*, 403–405.
(22) Clague, M. J.; Wishnok, J. S.; Marletta, M. A. *Biochemistry* **1997**, *36*, 14465–14473.
(23) Rosen, G. M.; Tsai, P.; Pou, S. *Chem. Rev.* **2002**, *102*, 1191–1199.
(24) Crane, B. R.; Arvai, A. S.; Ghosh, S.; Getzoff, E. D.; Stuehr, D. J.; Tainer, J. A. *Biochemistry* **2000**, *39*, 4608–4621.
(25) Woodward, J. J.; Chang, M. M.; Martin, N. I.; Marletta, M. A. *J. Am. Chem. Soc.* **2009**, *131*, 297–305.
(26) Cho, K.-B.; Derat, E.; Shaik, S. *J. Am. Chem. Soc.* **2007**, *129*, 3182–3188.
(27) Robinet, J. J.; Cho, K. B.; Gauld, J. W. *J. Am. Chem. Soc.* **2008**, *130*, 3328–3334.
(28) de Visser, S. P.; Tan, L. S. *J. Am. Chem. Soc.* **2008**, *130*, 12961–12974.
(29) Averill, B. A. *Chem. Rev.* **1996**, *96*, 2951–2964.
(30) Ferguson, S. J. *Curr. Opin. Chem. Biol.* **1998**, *2*, 182–193.
(31) Richardson, D. J.; Watmough, N. J. *Curr. Opin. Chem. Biol.* **1999**, *3*, 207–219.
(32) Moura, I.; Moura, J. J. G. *Curr. Opin. Chem. Biol.* **2001**, *5*, 168–175.
(33) Fülöp, V.; Moir, J. W. B.; Ferguson, S. J.; Hajdu, J. *Cell* **1995**, *81*, 369.
(34) Williams, P. A.; Fülöp, V.; Garman, E. F.; Saunders, N. F. W.; Ferguson, S. J.; Hajdu, J. *Nature* **1997**, *389*, 406.
(35) Nasri, H.; Wang, Y.; Hanh, H. B.; Scheidt, W. R. *J. Am. Chem. Soc.* **1991**, *113*, 717–719.
(36) Ranghino, G.; Scorza, E.; Sjögren, T.; Williams, P. A.; Ricci, M.; Hajdu, J. *Biochemistry* **2000**, *39*, 10958–10966.
(37) Martí, M. A.; Crespo, A.; Bari, S. E.; Doctorovich, F. A.; Estrin, D. A. *J. Phys. Chem. B* **2004**, *108*, 18073–18080.
(38) Nasri, H.; E., M. K.; Krebs, C.; Huynh, B. H.; Scheidt, W. R. *J. Am. Chem. Soc.* **2000**, *122*, 10795–10804.
(39) Haldane, J. *J. Hyg.* **1901**, *1*, 115–122.
(40) Brooks, J. *Proc. R. Soc. Med.* **1937**, *123*, 368–382.
(41) Møller, J. K. S.; Skibsted, L. H. *Chem. Rev.* **2002**, *102*, 1167–1178.
(42) Gladwin, M. T.; Grubina, R.; Doyle, M. P. *Acc. Chem. Res.* **2009**, *42*, 157–167.
(43) Gladwin, M. T.; Schechter, A. N.; Kim-Shapiro, D. B.; Patel, R. P.; Hogg, N.; Shiva, S.; Cannon, R. O., III; Kelm, M.; Wink, D. A.; Espey, M. G.; Oldfield, E. H.; Pluta, R. M.; Freeman, B. A.; Lancaster, J. R., Jr.; Feelisch, M.; Lundberg, J. O. *Nat. Chem. Biol.* **2005**, *1*, 308–314.
(44) Huang, Z.; Shiva, S.; Kim-Shapiro, D. B.; Patel, R. P.; Ringwood, L. A.; Irby, C. E.; Huang, K. T.; Ho, C.; Hogg, N.; Schechter, A. N.; Gladwin, M. T. *J. Clin. Invest.* **2005**, *115*, 2099–2107.
(45) Huang, K. T.; Keszler, A.; Patel, N.; Patel, R. P.; Gladwin, M. T.; Kim-Shapiro, D. B.; Hogg, N. *J. Biol. Chem.* **2005**, *280*, 31126–31131.
(46) Feelisch, M.; Fernandez, B. O.; Bryan, N. S.; Garcia-Saura, M. F.; Bauer, S.; Whitlock, D. R.; Ford, P. C.; Janero, D. R.; Rodriguez, J.; Ashrafian, H. *J. Biol. Chem.* **2008**, *283*, 33927–33934.
(47) Basu, S.; Grubina, R.; Huang, J.; Conradie, J.; Huang, Z.; Jeffers, A.; Jiang, A.; He, X.; Azarov, I.; Seibert, R.; Mehta, A.; Patel, R.; King, S. B.; Hogg, N.; Ghosh, A.; Gladwin, M. T.; Kim-Shapiro, D. B. *Nat. Chem. Biol.* **2007**, *3*, 785–794.
(48) Angelo, M.; Singel, D. J.; Stamler, J. S. *Proc. Natl. Acad. Sci. U.S.A.* **2006**, *103*, 8366–8371.
(49) Gow, A. J.; Stamler, J. S. *Nature* **1998**, *391*, 169–173.
(50) Singel, D. J.; Stamler, J. S. *Annu. Rev. Physiol.* **2005**, *67*, 99–145.
(51) Isbell, T. S.; Sun, C.-W.; Wu, L.-C.; Teng, X.; Vitturi, D. A.; Branch, B. G.; Kevil, C. G.; Peng, N.; Wyss, J. M.; Ambalavanan, N.; Schwiebert, L.; Ren, J.; Pawlik, K. M.; Renfrow, M. B.; Patel, R. P.; Townes, T. M. *Nat. Med.* **2008**, *14*, 773–777.
(52) Palmer, R. M.; Ferrige, A. G.; Moncada, S. *Nature* **1987**, *327*, 524–526.
(53) Ignarro, L. J.; Buga, G. M.; Wood, K. S.; Byrns, R. E.; Chaudhuri, G. *Proc. Natl. Acad. Sci. U.S.A.* **1987**, *84*, 9265–9269.
(54) Garbers, D. L.; Lowe, D. G. *J. Biol. Chem.* **1994**, *269*, 30741–30744.
(55) Zhao, Y.; Hoganson, C.; Babcock, G. T.; Marletta, M. A. *Biochemistry* **1998**, *37*, 12458–12464.
(56) Zhao, Y.; Brandish, P. E.; Ballou, D. P.; Marletta, M. A. *Proc. Natl. Acad. Sci. U.S.A.* **1999**, *96*, 14753–14758.
(57) Ballou, D. P.; Zhao, Y.; Brandish, P. E.; Marletta, M. A. *Proc. Natl. Acad. Sci. U.S.A.* **2002**, *99*, 12097–12101.
(58) Karow, D. S.; Pan, D.; Tran, R.; Pellicena, P.; Presley, A.; Mathies, R. A.; Marletta, M. A. *Biochemistry* **2004**, *43*, 10203–10211.
(59) Boon, E. M.; Marletta, M. A. *J. Inorg. Biochem.* **2005**, *99*, 892–902.
(60) Gilles-Gonzalez, M.-A.; Gonzales, G. *J. Inorg. Biochem.* **2005**, *99*, 1–22.
(61) Wyllie, G. R. A.; Schulz, C. E.; Scheidt, W. R. *Inorg. Chem.* **2003**, *42*, 5722–5734.
(62) Praneeth, V. K. K.; Neese, F.; Lehnert, N. *Inorg. Chem.* **2005**, *44*, 2570–2572.

accompanied by large structural changes of the enzyme, which activates the catalytic site of sGC for the conversion of guanosine triphosphate (GTP) to the secondary messenger cyclic guanosine monophosphate (cGMP). Recently, evidence has been presented that sGC has a second, lower-affinity binding site for NO, but the nature of this binding site is unclear.[57,69] Cytochrome $c'$, which is an unusual heme protein found in different bacteria, exhibits a similar 6C to 5C transition upon NO binding to the ferrous heme active site and has been used as a model for sGC.[70−73]

**Biological NO Transport.** The identification of small heme proteins, called nitrophorins, in the saliva of certain blood-sucking insects in the early 1990s that function as transporters for NO was certainly a surprise.[74,75] The first protein of this class was found in *Rhodnius prolixus* (the triatomid bug). The saliva of this insect contains four nitrophorin isozymes designated as rNp1−rNp4,[76] which form corresponding 6C ferric heme-nitrosyl complexes with proximal His coordination.[77−80] When the victim is bitten by *R. prolixus*, the nitrophorins are injected into the wound as part of the insect's saliva. Because of the lower concentration of NO in the area of the bite (dilution), and triggered by an increase in the pH, NO is then released into the wound,[74,81−83] activating sGC and inducing vasodilation, and, hence, causing an increase in blood flow via the victim's natural blood pressure control mechanism (*vide supra*). A few years after the discovery of the rNp protein family, it was found that the saliva of the blood-sucking insect *Cimex lectularius* (the common bedbug) also contains a nitrophorin,[84] which is designated as cNP.[85] The active site corresponds to a ferric heme with axial cysteine (Cys) coordination. Binding of NO to cNP then generates a corresponding 6C ferric heme-nitrosyl complex. The fact that the nitrophorins from both *R. prolixus* and *C. lectularius* transport NO in the ferric oxidation state is not arbitrary. Equilibrium binding constants $K_{eq}$ of NO to ferric hemes are in the range of $10^3-10^5\ M^{-1}$, which is several orders of magnitude lower compared to the corresponding ferrous complexes ($K_{eq} = 10^{10}-10^{12}\ M^{-1}$).[86−93] This difference is to a large extent due to increased dissociation rate constants in the ferric case. The ferric oxidation state is therefore required to allow for the release of NO from the nitrophorins, whereas the presence of either a His or thiolate (Cys) as the proximal ligand to heme does not seem to play an important role for the function of the nitrophorins.

**NO in Biological Catalysis.** Besides its central role in mammalian physiology, NO is also an important intermediate in bacterial and fungal dissimilatory denitrification.[30,31] Here, NO is produced by the reduction of nitrite (*vide supra*) and then further reduced to nitrous oxide ($N_2O$) by the NO reductase (NOR) family of enzymes.[94,95] In the process of NO biosynthesis by NOS or heme $cd_1$ NIR, 6C ferric heme-nitrosyl species are generated as enzyme−product complexes. As in the case of the nitrophorins, the ferric oxidation state is critical to ensuring that NO is readily lost from the heme center to complete the catalytic cycle. Interestingly, this lability is in contrast to the spectroscopically observed strong Fe−NO bonds in ferric heme-nitrosyls, as is evident from their large Fe−NO stretching frequencies. This puzzling contradiction is explained in Section C.1.

The next step in the denitrification cycle, i.e., the reduction of NO to $N_2O$ catalyzed by NORs, is particularly interesting since heme-nitrosyls serve as the reactive species in this case. Bacterial NO reductase (NorBC) is found in denitrifying bacteria like *Pseudomonas stutzeri* that live in terrestrial soil.[94] Detailed analyses

(63) Praneeth, V. K. K.; Näther, C.; Peters, G.; Lehnert, N. *Inorg. Chem.* **2006**, *45*, 2795–2811.
(64) Paulat, F.; Berto, T. C.; DeBeer George, S.; Goodrich, L. E.; Praneeth, V. K. K.; Sulok, C. D.; Lehnert, N. *Inorg. Chem.* **2008**, *47*, 11449–11451.
(65) Berto, T. C.; Praneeth, V. K. K.; Goodrich, L. E.; Lehnert, N. *J. Am. Chem. Soc.* **2009**, *131*, 17116–17126.
(66) Lehnert, N. Electron Paramagnetic Resonance and Low-Temperature Magnetic Circular Dichroism Spectroscopy of Ferrous Heme Nitrosyls. In *The Smallest Biomolecules: Diatomics and Their Interactions with Heme Proteins*; Ghosh, A., Ed.; Elseviere: Amsterdam, The Netherlands, 2008; pp 147−171.
(67) Praneeth, V. K. K.; Haupt, E.; Lehnert, N. *J. Inorg. Biochem.* **2005**, *99*, 940−948 (Erratum: p 1744).
(68) Yoshimura, T. *Inorg. Chim. Acta* **1982**, *57*, 99–105.
(69) Cary, S. P. L.; Winger, J. A.; Derbyshire, E. R.; Marletta, M. A. *Trends Biochem. Sci.* **2006**, *31*, 231–239.
(70) Usov, O. M.; Choi, P. S.-T.; Shapleigh, J. P.; Scholes, C. P. *J. Am. Chem. Soc.* **2006**, *128*, 5021–5032.
(71) Martí, M. A.; Capece, L.; Crespo, A.; Doctorovich, F.; Estrin, D. A. *J. Am. Chem. Soc.* **2005**, *127*, 7721–7728.
(72) Pixton, D. A.; Petersen, C. A.; Franke, A.; van Eldik, R.; Garton, E. M.; Andrew, C. R. *J. Am. Chem. Soc.* **2009**, *131*, 4846–4853.
(73) Barbieri, S.; Murphy, L. M.; Sawers, R. G.; Eady, R. R.; Hasnain, S. S. *J. Biol. Inorg. Chem.* **2008**, *13*, 531–540.
(74) Ribeiro, J. M. C.; Hazzard, J. M. H.; Nussenzveig, R. H.; Champagne, D. E.; Walker, F. A. *Science* **1993**, *260*, 539–541.
(75) Moncada, S.; Martin, J. F. *Lancet* **1993**, *341*, 1511.
(76) Walker, F. A. *J. Inorg. Biochem.* **2005**, *99*, 216–236.
(77) Weichsel, A.; Andersen, J. F.; Champagne, D. E.; Walker, F. A.; Montfort, W. R. *Nat. Struct. Biol.* **1998**, *5*, 304–309.
(78) Roberts, S. A.; Weichsel, A.; Qiu, Y.; Shelnutt, J. A.; Walker, F. A.; Montfort, W. R. *Biochemistry* **2001**, *40*, 11327–11337.
(79) Weichsel, A.; Andersen, J. F.; Roberts, S. A.; Montfort, W. R. *Nat. Struct. Biol.* **2000**, *7*, 551–554.
(80) Ding, X. D.; Weichsel, A.; Andersen, J. F.; Shokhireva, T. K.; Balfour, C.; Pierik, A. J.; Averill, B. A.; Montfort, W. R.; Walker, F. A. *J. Am. Chem. Soc.* **1999**, *121*, 128–138.
(81) Andersen, J. F.; Champagne, D. E.; Weichsel, A.; Ribeiro, J. M. C.; Balfour, C. A.; Dress, V.; Montfort, W. R. *Biochemistry* **1997**, *36*, 4423–4428.
(82) Andersen, J. F.; Ding, X. D.; Balfour, C.; Shokhireva, T. K.; Champagne, D. E.; Walker, F. A.; Montfort, W. R. *Biochemistry* **2000**, *39*, 10118–10131.
(83) Martí, M. A.; Lebrero, M. C. G.; Roitberg, A. E.; Estrin, D. A. *J. Am. Chem. Soc.* **2008**, *130*, 1611–1618.
(84) Valenzuela, J. G.; Ribeiro, J. M. C. *J. Exp. Biol.* **1998**, *201*, 2659–2664.
(85) Weichsel, A.; Maes, E. M.; Andersen, J. F.; Valenzuela, J. G.; Shokhireva, T. K.; Walker, F. A.; Montfort, W. R. *Proc. Natl. Acad. Sci. U.S.A.* **2005**, *102*, 594–599.
(86) Antonini, E.; Brunori, M.; Wyman, J.; Noble, R. W. *J. Biol. Chem.* **1966**, *241*, 3236–3238.
(87) Cassoly, R.; Gibson, Q. H. *J. Mol. Biol.* **1975**, *91*, 301–313.
(88) Sharma, V. S.; Traylor, T. G.; Gardiner, R.; Mizukami, H. *Biochemistry* **1987**, *26*, 3837–3843.
(89) Traylor, T. G.; Sharma, V. S. *Biochemistry* **1992**, *31*, 2847–2849.
(90) Hoshino, M.; Ozawa, K.; Seki, H.; Ford, P. C. *J. Am. Chem. Soc.* **1993**, *115*, 9568–9575.
(91) Cooper, C. E. *Biochim. Biophys. Acta* **1999**, *1411*, 290–309.
(92) Lim, M. D.; Lorkovic, I. M.; Ford, P. C. *J. Inorg. Biochem.* **2005**, *99*, 151–165.
(93) Ivanovic-Burmazovic, I.; van Eldik, R. *J. Chem. Soc., Dalton Trans.* **2008**, 5259–5275.
(94) Zumft, W. G. *J. Inorg. Biochem.* **2005**, *99*, 194–215.
(95) Daiber, A.; Shoun, H.; Ullrich, V. *J. Inorg. Biochem.* **2005**, *99*, 185–193.

of the amino acid sequences of NorBCs of different organisms[96−99] and spectroscopic investigations[100−102] have shown that these enzymes are closely related to the cytochrome *c* oxidases (CCOs).[103] The active sites of the CCOs available from several crystal structures,[104−107] as shown in Figure 1A,[106] therefore constitute blueprints for the active sites of the NorBCs, where crystallographic data are still lacking. However, in NorBC, the copper ion ($Cu_B$) is replaced by a nonheme iron ($Fe_B$).[100,101] The molecular mechanism of the NorBCs is not well understood. Electron paramagnetic resonance (EPR) spectroscopic investigations under turnover conditions revealed the formation of a "high-spin" nonheme ferrous nitrosyl with a $S = {}^3/_2$ ground state.[101] Vibrational data indicate binding of a second molecule of NO to the ferrous heme,[108,109] in agreement with the extremely large association constants of hemes for NO.[91] On the basis of these findings, the mechanism in Figure 1B has been proposed.[110] In this case, two molecules of NO are bound to the diferrous active site, and then a radical-type N−N bond formation is postulated. After the release of $N_2O$, the two ferric iron centers are bridged by an oxo group.[100,110−112] However, no intermediate of this mechanism has ever been observed, which renders its central part, the N−N coupling, speculative. From density functional theory (DFT) calculations[113] and in analogy to the proposed mechanism for the reduction of NO by CCO,[114−116] a bridging hyponitrite complex is anticipated as the intermediate. Alternative mechanisms have also been proposed in which, for example, only one of the two metal sites (heme or nonheme) reacts directly with NO, whereas the other metal only serves as an electron reservoir.[94,113,117−120] Another important question, the coordination number of the heme-nitrosyl, is an additional issue (see Section B.5).[63,102,121] Model complex studies present further evidence that the catalytically active species indeed corresponds to the ferrous heme (NO)/nonheme (NO) dinitrosyl complex, in agreement with Figure 1B.[122−124]

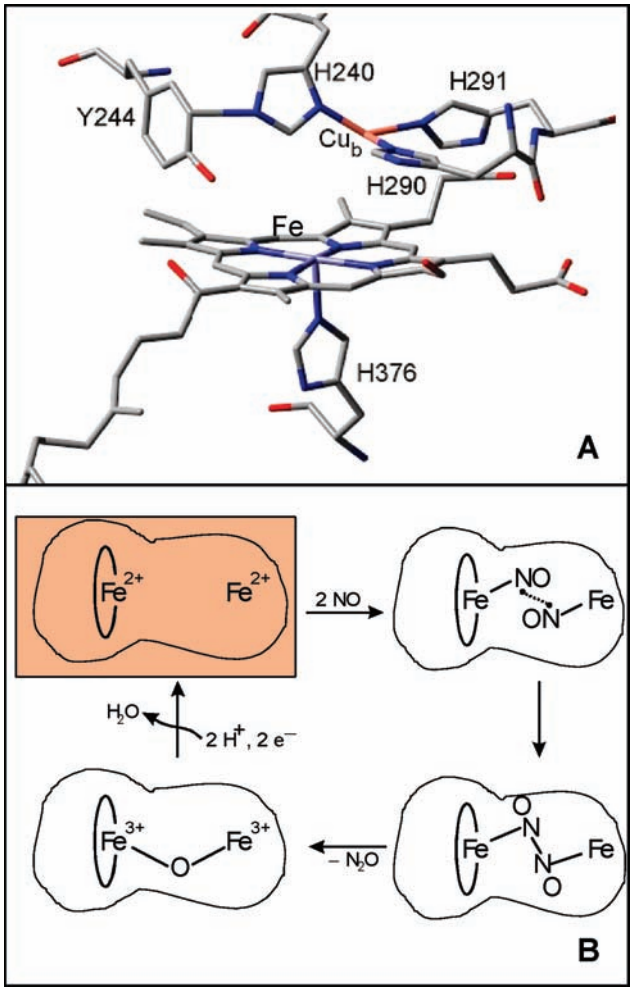


**Figure 1.** (A) Crystal structure of the active site of mitochondrial CCO.[106] (B) Proposed mechanism for NorBC.[110]

(96) van der Oost, J.; de Boer, A. P. N.; de Gier, J.-W. L.; Zumft, W. G.; Stouthamer, A. H.; van Spanning, R. J. M. *FEMS Microbiol. Lett*. **1994**, *121*, 1–10.
(97) Saraste, M.; Castresana, J. *FEBS Lett*. **1994**, *341*, 1–4.
(98) Arai, H.; Igarashi, Y.; Kodama, T. *Biochim. Biophys. Acta* **1995**, *1261*, 279–284.
(99) de Boer, A. P. N.; van der Oost, J.; Reijnders, W. N. M.; Westerhoff, H. V.; Stouthamer, A. H.; van Spanning, R. J. M. *Eur. J. Biochem*. **1996**, *242*, 592–600.
(100) Cheesman, M. R.; Zumft, W. G.; Thomson, A. J. *Biochemistry* **1998**, *37*, 3994–4000.
(101) Hendriks, J.; Warne, A.; Gohlke, U.; Haltia, T.; Ludovici, C.; Lübben, M.; Saraste, M. *Biochemistry* **1998**, *37*, 13102–13109.
(102) Moënne-Loccoz, P.; de Vries, S. *J. Am. Chem. Soc*. **1998**, *120*, 5147–5152.
(103) Grönberg, K. L. C.; Roldán, M. D.; Prior, L.; Butland, G.; Cheesman, M. R.; Richardson, D. J.; Spiro, S.; Thomson, A. J.; Watmough, N. J. *Biochemistry* **1999**, *38*, 13780–13786.
(104) Tsukihara, T.; Aoyama, H.; Yamashita, E.; Tomizaki, T.; Yamaguchi, H.; Shinzawa-Itoh, K.; Nakashima, R.; Yaono, R.; Yoshikawa, S. *Science* **1995**, *269*, 1069–1074.
(105) Iwata, S.; Ostermeier, C.; Ludwig, B.; Michel, H. *Nature* **1995**, *376*, 660–669.
(106) Tsukihara, T.; Aoyama, H.; Yamashita, E.; Tomizaki, T.; Yamaguchi, H.; Shinzawa-Itoh, K.; Nakashima, R.; Yaono, R.; Yoshikawa, S. *Science* **1996**, *272*, 1136–1144.
(107) Yoshikawa, S.; Shinzawa-Itoh, K.; Yamashita, E.; Tsukihara, T. Mitochondrial cytochrome c oxidase. In *Handbook of Metalloproteins*; Messerschmidt, A., Huber, R., Poulos, T., Wieghardt, K., Eds.; Wiley: Chichester, England, 2001; Vol. *1*.
(108) Pinakoulaki, E.; Gemeinhardt, S.; Saraste, M.; Varotsis, C. *J. Biol. Chem*. **2002**, *277*, 23407–23413.
(109) Lu, S.; Suharti; de Vries, S.; Moënne-Loccoz, P. *J. Am. Chem. Soc*. **2004**, *126*, 15332–15333.
(110) Girsch, P.; de Vries, S. *Biochim. Biophys. Acta* **1997**, *1318*, 202–216.
(111) Martens, C. F.; Murthy, N. N.; Obias, H. V.; Karlin, K. D. *Chem. Commun*. **1996**, 629–630.
(112) Moënne-Loccoz, P.; Richter, O.-M. H.; Huang, H.; Wasser, I. M.; Ghiladi, R. A.; Karlin, K. D.; de Vries, S. *J. Am. Chem. Soc*. **2000**, *122*, 9344–9345.
(113) Blomberg, L. M.; Blomberg, M. R. A.; Siegbahn, P. E. M. *Biochim. Biophys. Acta* **2006**, *1757*, 240–252.
(114) Ohta, T.; Kitagawa, T.; Varotsis, C. *Inorg. Chem*. **2006**, *45*, 3187–3190.
(115) Blomberg, L. M.; Blomberg, M. R. A.; Siegbahn, P. E. M. *Biochim. Biophys. Acta* **2006**, *1757*, 31–46.
(116) Varotsis, C.; Ohta, T.; Kitagawa, T.; Soulimane, T.; Pinakoulaki, E. *Angew. Chem., Int. Ed*. **2007**, *46*, 2210–2214.
(117) Butler, C. S.; Seward, H. E.; Greenwood, C.; Thomson, A. J. *Biochemistry* **1997**, *36*, 16259–16266.
(118) Watmough, N. J.; Cheesman, M. R.; Butler, C. S.; Little, R. H.; Greenwood, C.; Thomson, A. J. *J. Bioenerg. Biomembr*. **1998**, *30*, 55–62.
(119) Lin, R.; Farmer, P. J. *J. Am. Chem. Soc*. **2001**, *123*, 1143–1150.
(120) Hayashi, T.; Lin, M. T.; Ganesan, K.; Chen, Y.; Fee, J. A.; Gennis, R. B.; Moënne-Loccoz, P. *Biochemistry* **2009**, *48*, 883–890.
(121) Pinakoulaki, E.; Ohta, T.; Soulimane, T.; Kitagawa, T.; Varotsis, C. *J. Am. Chem. Soc*. **2005**, *127*, 15161–15167.
(122) Wasser, I. M.; Huang, H.; Moënne-Loccoz, P.; Karlin, K. D. *J. Am. Chem. Soc*. **2005**, *127*, 3310–3320.
(123) Collman, J. P.; Yang, Y.; Dey, A.; Decreau, R. A.; Ghosh, S.; Ohta, T.; Solomon, E. I. *Proc. Natl. Acad. Sci. U.S.A*. **2008**, *105*, 15660–15665.
(124) Collman, J. P.; Dey, A.; Yang, Y.; Decreau, R. A.; Ohta, T.; Solomon, E. I. *J. Am. Chem. Soc*. **2008**, *130*, 16498–16499.

However, no intermediates of the reaction were detected, and catalytic turnover was not achieved. Recently, Lu and co-workers have succeeded in engineering a nonheme iron binding site into the distal pocket of Mb that provides the $His_3Glu$ ligand environment anticipated for $Fe_B$.[125] Interestingly, the diiron form of this protein is, in fact, catalytically active in the reduction of NO to $N_2O$, although at a very slow rate. The results show that Glu is required for stable coordination of $Fe_B$, implying that a similar carboxylate side chain might bind the $Fe_B$ center in NorBC.

Fungal NOR is a member of the P450 family and is therefore designated as P450nor. Several crystal structures of the enzyme from *Fusarium oxysporum* have been determined. These show a heme *b* with axial cysteinate coordination, as illustrated in Figure 2A.[126−128] Binding of one molecule of NO to the catalytically active, ferric form then leads to a 6C ferric heme-nitrosyl as the first intermediate.[129−133] Stopped-flow kinetic investigations have demonstrated that this species undergoes two-electron reduction with NADH, forming the so-called "intermediate I",[130] which corresponds to an iron(II)-nitroxyl or $Fe^I$−NO complex.[134] The reaction of this species with a second molecule of NO then closes the catalytic cycle.[130] The most important question with respect to this mechanism governs the exact nature of intermediate I.[95] Recently, strong evidence has been presented that this species is actually protonated.[135,136] Model complex studies on P450nor suffer from the instability of the Fe−S bond in ferric heme-nitrosyls (*vide infra*).[137] Only two stable ferric heme-thiolate NO model complexes have been synthesized so far, but these compounds are incapable of catalyzing the reduction of NO.[138,139]

The interaction of NO with cytochrome P450s and the potential implications for human physiology have, in general, gained attention in recent years. As one would expect, NO is able to reversibly inhibit cytochrome P450s by binding to their heme active sites.[140,141] This might also contribute to the antimicrobial effect of NO, as exploited by the human immune system (*vide supra*) via inhibition of cytochrome P450s in pathogens.[142]

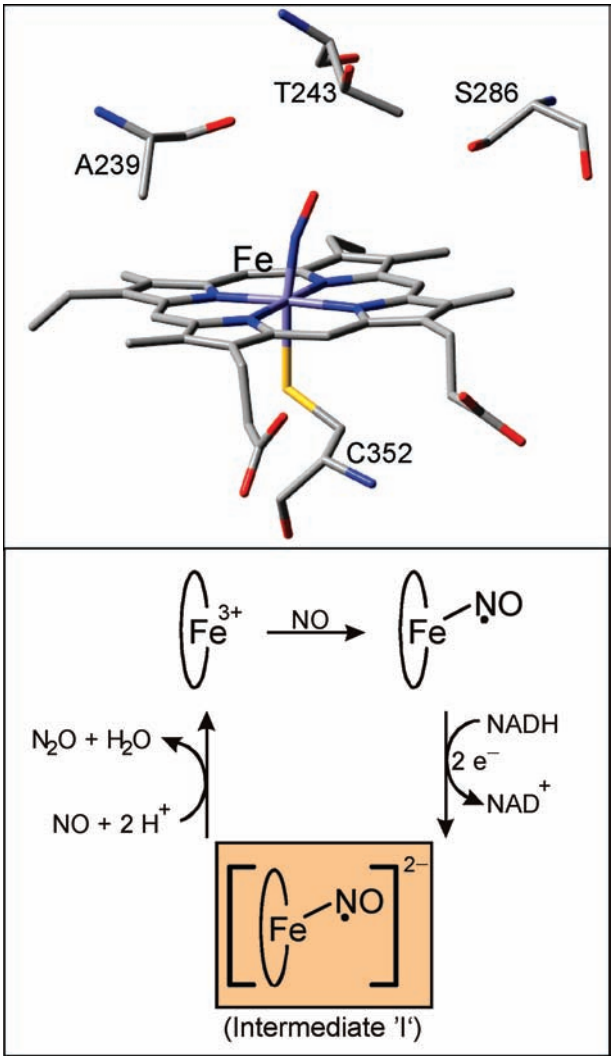


**Figure 2.** (A, top) Crystal structure of the ferric active site of P450nor with bound NO.[127] (B, bottom) Proposed mechanism.[130]

**Model Systems.** Because many of the biologically important functions and transformations of NO are mediated by heme proteins, many corresponding model complexes have been synthesized and structurally and spectroscopically characterized in detail.[143−146] In particular, tetraphenylporphyrin ($H_2TPP$), octaethylporphyrin ($H_2OEP$), and protoporphyrin IX diester ($H_2PPDE$),

(125) Yeung, N.; Lin, Y. W.; Gao, Y. G.; Zhao, X.; Russell, B. S.; Lei, L.; Miner, K. D.; Robinson, H.; Lu, Y. *Nature* **2009**, *462*(7276), 1079–1082.
(126) Park, S.-Y.; Shimizu, H.; Adachi, S.; Nagagawa, A.; Tanaka, I.; Nakahara, K.; Shoun, H.; Obayashi, E.; Nakamura, H.; Iizuka, T.; Shiro, Y. *Nat. Struct. Biol.* **1997**, *4*, 827–832.
(127) Shimizu, H.; Park, S.-Y.; Gomi, Y.; Arakawa, H.; Nakamura, H.; Adachi, S.-I.; Obayashi, E.; Iizuka, T.; Shoun, H.; Shiro, Y. *J. Biol. Chem.* **2000**, *275*, 4816–4826.
(128) Shimizu, H.; Park, S.-Y.; Shiro, Y.; Adachi, S.-I. *Acta Crystallogr., Sect. D* **2002**, *58*, 81.
(129) Nakahara, K.; Tanimoto, T.; Hatano, K.; Usuda, K.; Shoun, H. *J. Biol. Chem.* **1993**, *268*, 8350–8355.
(130) Shiro, Y.; Fujii, M.; Iizuka, T.; Adachi, S.; Tsukamoto, K.; Nakahara, K.; Shoun, H. *J. Biol. Chem.* **1995**, *270*, 1617–1623.
(131) Shiro, Y.; Fujii, M.; Isogai, Y.; Adachi, S.; Iizuka, T.; Obayashi, E.; Makino, R.; Nakahara, K.; Shoun, H. *Biochemistry* **1995**, *34*, 9052–9058.
(132) Obayashi, E.; Tsukamoto, K.; Adachi, S.; Takahashi, S.; Nomura, M.; Iizuka, T.; Shoun, H.; Shiro, Y. *J. Am. Chem. Soc.* **1997**, *119*, 7807–7816.
(133) Singh, U. P.; Obayashi, E.; Takahashi, S.; Iizuka, T.; Shoun, H.; Shiro, Y. *Biochim. Biophys. Acta* **1998**, *1384*, 103–111.
(134) Obayashi, E.; Takahashi, S.; Shiro, Y. *J. Am. Chem. Soc.* **1998**, *120*, 12964–12965.
(135) Daiber, A.; Nauser, T.; Takaya, N.; Kudo, T.; Weber, P.; Hultschig, C.; Shoun, H.; Ullrich, V. *J. Inorg. Biochem.* **2002**, *88*, 343–352.
(136) Lehnert, N.; Praneeth, V. K. K.; Paulat, F. *J. Comput. Chem.* **2006**, *27*, 1338–1351.
(137) Franke, A.; Stochel, G.; Suzuki, N.; Higuchi, T.; Okuzono, K.; van Eldik, R. *J. Am. Chem. Soc.* **2005**, *127*, 5360–5375.
(138) Suzuki, N.; Higuchi, T.; Urano, Y.; Kikuchi, K.; Uchida, T.; Mukai, M.; Kitagawa, T.; Nagano, T. *J. Am. Chem. Soc.* **2000**, *122*, 12059–12060.
(139) Xu, N.; Powell, D. R.; Cheng, L.; Richter-Addo, G. B. *Chem. Commun.* **2006**, 2030–2032.
(140) Wink, D. A.; Osawa, Y.; Darbyshire, J. F.; Jones, C. R.; Eshenaur, S. C.; Nims, R. W. *Arch. Biochem. Biophys.* **1993**, *300*, 115–123.
(141) Hanke, C. J.; Drewett, J. G.; Myers, C. R.; Campbell, W. B. *Endocrinology* **1998**, *139*, 4053–4060.
(142) Ouellet, H.; Lang, J.; Couture, M.; Ortiz de Montellano, P. R. *Biochemistry* **2009**, *48*, 863–872.
(143) Cheng, L.; Richter-Addo, G. B. Binding and Activation of Nitric Oxide by Metalloporphyrins and Heme. In *The Porphyrin Handbook*; Kadish, K. M., Smith, K. M., Guilard, R., Eds.; Academic Press: New York, 2000; Vol. *4*, Chapter 33, pp 219−291.
(144) Ford, P. C.; Lorkovic, I. M. *Chem. Rev.* **2002**, *102*, 993–1017.
(145) Wyllie, G. R. A.; Scheidt, W. R. *Chem. Rev.* **2002**, *102*, 1067–1090.
(146) Walker, F. A.; Simonis, U. Iron Porphyrin Chemistry. In *Encyclopedia of Inorganic Chemistry*, 2nd ed.; King, R. B., Ed.; John Wiley & Sons, Ltd.: Chichester, U.K., 2005; Vol. *IV*, pp 2390−2521.

**Scheme 1**

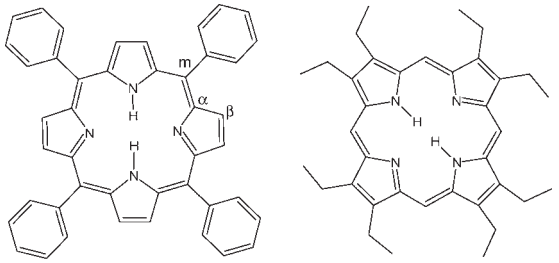


Tetraphenylporphyrin ($H_2$TPP)




Octaethylporphyrin ($H_2$OEP)

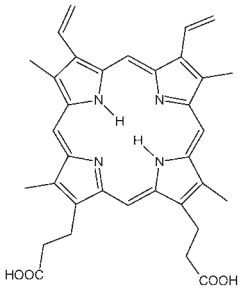


Protoporphyrin IX ($H_2$PP)

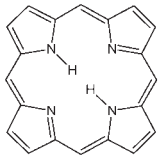


Porphine ($H_2$P)

as shown in Scheme 1, and their corresponding derivatives have been widely used. Studies of model systems are very useful to investigate and understand the fundamental chemistry of hemes with NO and its derivatives (termed $NO_x$ in the following; this includes nitrite, nitroxyl, peroxynitrite, etc.) and to structurally and spectroscopically characterize corresponding heme-$NO_x$ complexes.[92,145−151] This provides the foundation to identify, understand, and predict corresponding reactions in biological systems, to critically evaluate proposed mechanisms for heme-$NO_x$ interactions, and, based on the spectroscopic signatures of heme-$NO_x$ model complexes, to identify corresponding species in proteins. Model systems can also be used to investigate reaction mechanisms under conditions that cannot be applied to biological species, for example, low reaction temperatures (−80 °C) or strictly water-free environments, and in this way, intermediates that are impossible to observe in the actual enzymatic reactions might be accessible. This is particularly true for proton-dependent processes. Finally, model complexes can form the basis for the development of new therapeutics.[148] In summary, model complex studies can contribute much to the understanding of biologically important processes, and the insight that can be obtained is only limited by our creativities and abilities as (bioinorganic) chemists. The ultimate achievement in this respect is to build a *functional* model that is able to carry out the same reaction as the corresponding protein. Because a great way to understand how a machine works is not just to take it apart and look at each of its components, *it is to actually build your own*.

(147) Ford, P. C. *Inorg. Chem.* **2010**, *49*, accepted for publication.
(148) Su, J.; Groves, J. T. *Inorg. Chem.* **2010**, *49*, accepted for publication.
(149) Heinecke, J.; Ford, P. C. *Coord. Chem. Rev.* **2010**, *254*, 235–247.
(150) Schopfer, M. P.; Mondal, B.; Lee, D.-H.; Sarjeant, A. A. N.; Karlin, K. D. *J. Am. Chem. Soc.* **2009**, *131*, 11304–11305.
(151) Collman, J. P.; Boulatov, R.; Sunderland, C. J.; Fu, L. *Chem. Rev.* **2004**, *104*, 561–588.

## B. Ferrous Heme-Nitrosyls

### B.1. 5C Ferrous Heme-Nitrosyls.

**Geometric and Spectroscopic Properties.** 5C ferrous heme-nitrosyls of the general formula [Fe(Porphyrin)(NO)] in proteins and model complexes exhibit low-spin ground states of $S = {}^1/_2$ total spin. The geometries of the Fe−N−O units in these compounds do not show much variation as a function of the porphyrin ligand, as indicated in Table 1. The general (average) structural features of these species are summarized in Scheme 2, left.[61] Important structural parameters are short Fe−NO distances of ∼1.73 Å, bent Fe−N−O units of ∼140−145°, and a distinct displacement of the iron center from the porphyrin plane by ∼0.3 Å. High-resolution crystal structures of corresponding model complexes also reveal a slight tilting of the Fe−NO bond vector from the heme normal and an asymmetry of the Fe−N(pyrrole) bond distances, as indicated in Scheme 2.[152]

5C ferrous heme-nitrosyls exhibit characteristic EPR spectra with average $g$ values of about 2.10, 2.06, and 2.01 (see ref 66 for details). The spectrum of [Fe(TPP)(NO)] is shown in Figure 3, left, as an example. Single-crystal EPR measurements on the model complex [Fe(OEP)(NO)] have revealed that the principal axis of the minimum $g$ value, $g_{min}$, is closely aligned with the Fe−NO bond vector[153] and, therefore, corresponds to $g_z$ in the coordinate system shown in Scheme 3. With NO in the $xz$ plane, $g_{max}$ (∼2.1) is then equivalent to $g_y$ and $g_{mid}$ (∼2.06) corresponds to $g_x$. In addition, three strong hyperfine lines due to the presence of the $^{14}$N nucleus of NO are typically resolved on $g_{min}$, giving rise to the very characteristic EPR signal of 5C ferrous heme-nitrosyls, as shown in Figure 3, left. The three-line hyperfine pattern originates from the nuclear spin $I = 1$ of $^{14}$N. The $^{14}$N hyperfine tensor components, available for a few model systems, are quite isotropic in the 5C case, as discussed in ref 66.

Vibrational spectroscopy is another key technique to study ferrous heme-nitrosyls because the vibrational properties of these complexes are very sensitive to the coordination number, oxidation state, spin state, etc., of the metal. In general, the N−O stretching frequency $\nu$(N−O) is very intense in the IR spectra and, hence, is easily identified with this method. Resonance Raman and Nuclear Resonance Vibrational Spectroscopy (NRVS),[154,155] on the other hand, can be used to assign the Fe−NO stretching, $\nu$(Fe−NO), and the in-plane Fe−N−O bending, $\delta_{ip}$(Fe−N−O), modes. NRVS is particularly valuable in this respect because ferrous heme-nitrosyls are potentially photolabile and, in addition, $\nu$(Fe−NO) and $\delta_{ip}$(Fe−N−O) are usually very weak in the resonance Raman spectra of these compounds.[63,156] In contrast, NRVS is ideal for the identification of metal−ligand

(152) Scheidt, W. R.; Duval, H. F.; Neal, T. J.; Ellison, M. K. *J. Am. Chem. Soc.* **2000**, *122*, 4651–4659.
(153) Hayes, R. G.; Ellison, M. K.; Scheidt, W. R. *Inorg. Chem.* **2000**, *39*, 3665–3668.
(154) Sage, J. T.; Paxson, C.; Wyllie, G. R. A.; Sturhahn, W.; Durbin, S. M.; Champion, P. M.; Alp, E. E.; Scheidt, W. R. *J. Phys.: Condens. Matter* **2001**, *13*, 7707–7722.
(155) Sturhahn, W. *J. Phys.: Condens. Matter* **2004**, *16*, S497–S530.
(156) Ibrahim, M.; Xu, C.; Spiro, T. G. *J. Am. Chem. Soc.* **2006**, *128*, 16834–16845.

**Table 1.** Geometric and Vibrational Properties of Selected Five-Coordinate [Fe(Porphyrin)(NO)] Complexes in Model Systems and Proteins (See refs 80, 143, 145, and 206 for Additional Examples)

| molecule[a] | geometric parameters [Å][b] | | | | | vibrational frequencies [cm$^{-1}$] | | | | |
|---|---|---|---|---|---|---|---|---|---|---|
| | ΔFe−N | ΔN−O | ∠Fe−N−O | ΔFe−N$_P$ | ref | ν(N−O) | ν(Fe−NO) | δ$_{ip}$(Fe−N−O) | ref | condition |
| [Fe$^{II}$(OEP)(NO)] | | | | | | 1671 | 522[d] | 388[d] | 159 | KBr (N−O), solid |
| monoclinic (form I) | 1.722 | 1.167 | 144 | 2.004 | 152 | | | | | |
| triclinic (form II) | 1.731 | 1.168 | 143 | 2.010 | 152 | | | | | |
| [Fe$^{II}$(OEP)($^{15}$N$^{18}$O)] | | | | | | 1595 | 508[d] | 381[d] | 159 | |
| [Fe$^{II}$(TPP)(NO)][c] | 1.739 | 1.163 | 144 | 2.00 | 207 | 1697 | 532 | 371 | 63 | KBr |
| [Fe$^{II}$(TPP)($^{15}$N$^{18}$O)] | | | | | | 1625 | 515 | 365 | 63 | |
| [Fe$^{II}$(TPPBr$_8$)(NO)] | 1.75 | 1.42 | 146 | 1.986 | 168 | 1685 | | | 168 | KBr |
| [Fe$^{II}$(DPDME)(NO)] | 1.723 | 1.187 | 143 | 2.005 | 206 | 1651 | | | 206 | KBr |
| α-Hb$^{II}$−NO | 1.74 | 1.1 | 145 | | 208 | 1668[e] | | | 209 | buffer |
| sGC$^{II}$−NO | | | | | | 1681 | 521 | | 210 | buffer |
| [Fe$^{II}$(OEP)(NO)], form I (calcd: B3LYP/LanL2DZ) | 1.742 | 1.215 | 143 | 2.020 | 159 | 1615 | 503 | 403 | 159 | |
| [Fe$^{II}$(OEP)(NO)], form I (calcd: BP86/LanL2DZ*) | 1.687 | 1.190 | 144 | 2.023 | 159 | 1713 | 620 | 406 | 159 | |
| [Fe$^{II}$(P)(NO)] (calcd: BP86/TZVP) | 1.705 | 1.179 | 146 | 2.019 | 62 | 1703 | 595 | 427 | 62 | |
| [Fe$^{II}$(P)(NO)] (calcd: BP86/LanL2DZ*) | 1.688 | 1.188 | 144 | 2.021 | 159 | 1726 | 619 | 428 | 159 | |
| [Fe$^{II}$(P)(NO)] (calcd: B3LYP/TZVP) | 1.718 | 1.161 | 142 | 2.021 | 159 | 1790 | 585 | 444 | 159 | |
| [Fe$^{II}$(P)(NO)] (calcd: B3LYP/LanL2DZ*) | 1.712 | 1.169 | 141 | 2.020 | 159 | 1825 | 538 | 435 | 159 | |
| [Fe$^{II}$(P)(NO)] (calcd: B3LYP/LanL2DZ) | 1.742 | 1.212 | 143 | 2.019 | 63 | 1637 | 507 | 425 | 63 | |

[a] DPDME = deuteroporphyrin IX dimethyl ester$^{2-}$; P = Porphine$^{2-}$ ligand used for calculations. [b] The values for ΔFe−N$_P$ [Fe−N(porphyrin) distance] are averaged. [c] Triclinic, recorded at 33 K. [d] Determined from NRVS using $^{57}$Fe. Compared to natural abundance isotopes (n.a.i.) Fe, the modes ν(Fe−NO) and δ$_{ip}$(Fe−N−O) appear about 1−2 cm$^{-1}$ shifted to lower energy. [e] Determined for the inositol hexaphosphate complex of human Hb.

**Scheme 2.** General Structural Motifs of 5C [Fe(Porphyrin)(NO)] and 6C [Fe(Porphyrin)(L)(NO)] (L = N-Donor Ligand) Complexes (Reprinted with Permission from ref 61. Copyright 2003 American Chemical Society)




stretching vibrations since NRVS intensities are proportional to the amount of iron motion in a normal mode.[157,158] Figure 4, top, shows the NRVS spectra of the 5C complex [$^{57}$Fe(OEP)(NO)] (black line) and of the corresponding $^{15}$N$^{18}$O isotopic labeled compound (red line) as an example.[159] The NRVS data exhibit the Fe−NO stretch, ν(Fe−NO), at 522 cm$^{-1}$ and the in-plane Fe−N−O bend, δ$_{ip}$(Fe−N−O), at 388 cm$^{-1}$, which shift to 508 and 381 cm$^{-1}$ in the $^{15}$N$^{18}$O complex, respectively. From IR measurements, the N−O stretch is identified at 1671 cm$^{-1}$. These results are in good agreement with previous assignments for [Fe(TPP)(NO)][62,63] and other 5C model systems[160] and the 5C ferrous sGC-NO and Hb-NO adducts (cf. Table 1). In summary, typical vibrational energies for 5C ferrous heme-nitrosyls are 1670−1700 cm$^{-1}$ for ν(N−O) and 520−540 cm$^{-1}$ for ν(Fe−NO).

**Normal Coordinate Analysis.** In order to simulate the vibrational energies, isotope shifts, and NRVS VDOS intensities of these compounds and to derive force constants as representative descriptors of the Fe−NO and N−O bond strengths, we applied our quantum chemistry centered normal coordinate analysis (QCC-NCA).[63,161] Here, an initial set of force constants is generated from high-level DFT calculations, which serve as the initial guess for the following NCA. Only a few selected force constants are subsequently varied in order to reproduce the vibrational energies of the relevant subunit of the molecule, here the Fe−N−O unit. For example, the relatively small molecule [Fe(OEP)(NO)] already has ∼48 800 individual force constants (in $C_1$ symmetry). The QCC-NCA procedure elegantly circumvents the problem of having to invent all of these force constants by starting from a DFT-calculated force field. This avoids the arbitrariness of a conventional NCA, thereby improving the reliability of the NCA results.[161] Application of the QCC-NCA method to ferrous heme-nitrosyls is particularly important because the accuracy of the DFT calculations for the Fe−N−O subunit of these compounds is quite dissatisfactory (*vide infra*). However, these deviations can easily be corrected via the QCC-NCA approach. The QCC-NCA analysis yielded force constants of 12.15 and 2.94 mdyn/Å for the N−O and Fe−NO bonds in [Fe(OEP)(NO)][159] compared to 12.53 and 2.98 mdyn/Å for [Fe(TPP)(NO)],[63] indicating similar electronic properties of these complexes (cf. Table 2).[159]

**Electronic Structure.** The principal bonding scheme of Fe$^{II}$−NO adducts has been described by Enemark and

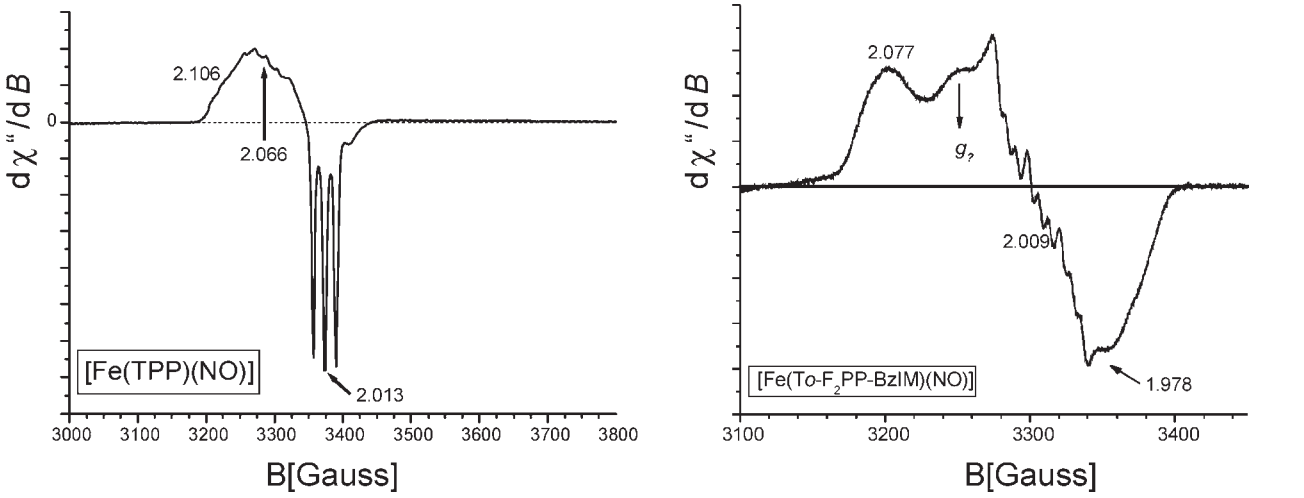


**Figure 3.** Left: EPR spectrum of the 5C complex [Fe(TPP)(NO)]. Reprinted with permission from ref 67. Copyright 2005 Elsevier. Right: EPR spectrum of the 6C complex [Fe(T*o*-$F_2$PP-BzIM)(NO)] using a porphyrin ligand with a covalently attached imidazole tail. Reprinted with permission from ref 65. Copyright 2009 American Chemical Society.

**Scheme 3.** General Coordinate System Applied to Heme-Nitrosyls in This Paper[a]

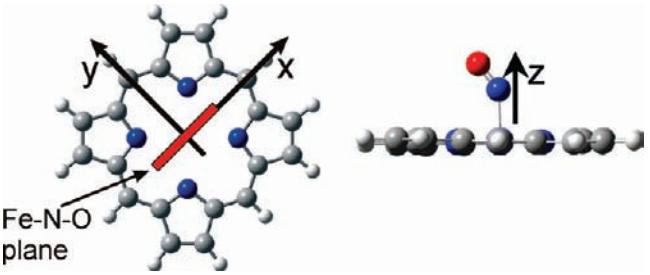


[a] In the case of ferrous heme-nitrosyls with bent Fe−N−O units, the NO ligand is located in the *xz* plane, as indicated on the left (red rectangle).

Feltham in their classic paper on the electronic structures of transition-metal nitrosyls.[162] These complexes were classified as $\{FeNO\}^7$, where the superscript "7" refers to the number of d electrons of the metal plus the one unpaired electron of NO (cf. Scheme 4, left). The general description of the electronic structure of $\{FeNO\}^7$ systems developed in this paper is also applicable to ferrous heme-nitrosyls and explains basic features of these compounds. However, the $\{FeNO\}^7$ formalism leaves room for a large variation of the electronic structure mediated by metal−ligand covalency: variation all of the way from an $Fe^{III}-NO^-$ extreme, on the one side, to an $Fe^{I}-NO^+$

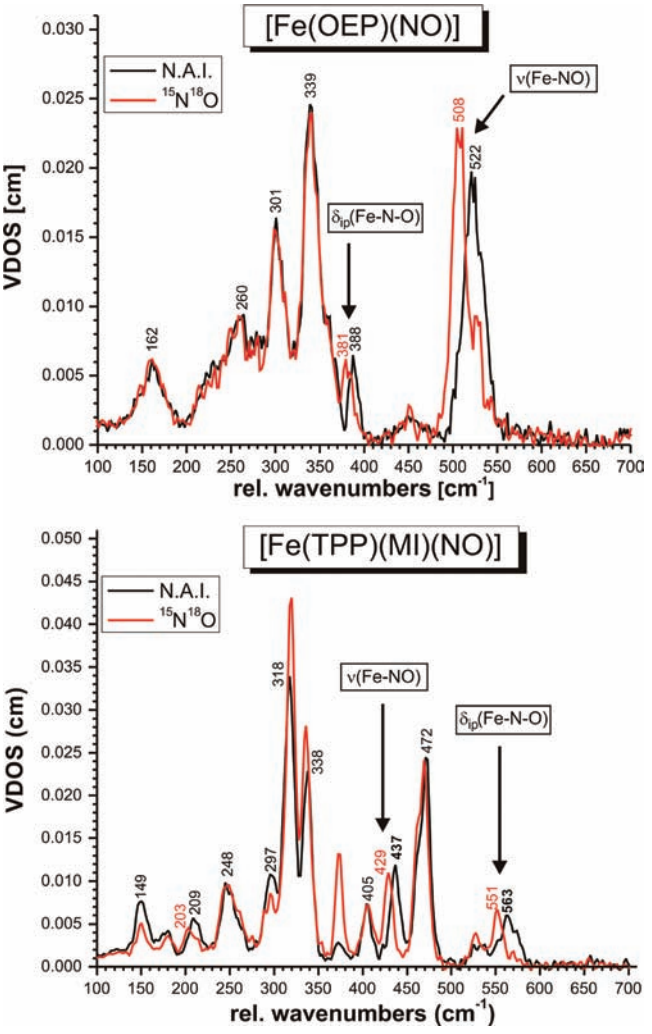


**Figure 4.** Vibrational density of states (VDOS) for powder samples of [$^{57}$Fe(OEP)(NO)] (top) and [$^{57}$Fe(TPP)(MI)(NO)] (bottom). Black: nai = natural abundance isotopes NO. Red: $^{15}N^{18}O$-labeled complex. Reprinted with permission from refs 159 and 64. Copyright 2010 and 2008, respectively, American Chemical Society.

(157) Scheidt, W. R.; Durbin, S. M.; Sage, J. T. *J. Inorg. Biochem.* **2005**, *99*, 60–71.
(158) Zeng, W.; Silvernail, N. J.; Scheidt, W. R.; Sage, J. T. Nuclear Resonance Vibrational Spectroscopy (NRVS). In *Applications of Physical Methods to Inorganic and Bioinorganic Chemistry, Encyclopedia of Inorganic Chemistry*; Scott, R. A., Lukehart, C. M., Eds.; John Wiley & Sons, Ltd.: Chichester, U.K., 2007; pp 1−21.
(159) Lehnert, N.; Galinato, M. G. I.; Paulat, F.; Richter-Addo, G. B.; Sturhahn, W.; Xu, N.; Zhao, J. *Inorg. Chem.* **2010**, *49*, ASAP.
(160) Leu, B. M.; Zgierski, M. Z.; Wyllie, G. R. A.; Scheidt, W. R.; Sturhahn, W.; Alp, E. E.; Durbin, S. M.; Sage, J. T. *J. Am. Chem. Soc.* **2004**, *126*, 4211–4227.
(161) Lehnert, N. Quantum Chemistry Centered Normal Coordinate Analysis (QCC-NCA): Routine Application of Normal Coordinate Analysis for the Simulation of the Vibrational Spectra of large Molecules. In *Computational Inorganic and Bioinorganic Chemistry*; Solomon, E. I., King, R. B., Scott, R. A., Eds.; John Wiley & Sons: Chichester, U.K., 2009; pp 123−140.
(162) Enemark, J. H.; Feltham, R. D. *Coord. Chem. Rev.* **1974**, *13*, 339–406.

**Table 2.** QCC-NCA Results for Five- and Six-Coordinate Heme-Nitrosyls in Comparison

| | vibrational frequency [$cm^{-1}$] [a] | | | force constant [mdyn/Å] | | | |
|---|---|---|---|---|---|---|---|
| method | $\nu$(N−O) | $\nu$(Fe−NO) | $\delta_{ip}$(Fe−N−O) [b] | $f_{N-O}$ | $f_{Fe-NO}$ | $f_{Fe-N-O}$ [c] | ref |
| [$^{57}$Fe(OEP)(NO)]: EXP. | 1671 (1595) | 522 (508) | 388 (381) | | | | 159 |
| [Fe(OEP)(NO)]: BP86/LanL2DZ* | 1712 | 620 | 414 | 12.798 | 3.854 | 0.469 | 159 |
| [$^{57}$Fe(OEP)(NO)]: QCC-NCA | 1671 (1598) | 522 (508) | 388 (381) | 12.148 | 2.938 | 0.346 | 159 |
| [Fe(TPP)(NO)]: EXP. | 1697 (1625) | 532 (515) | 371 (365) | | | | 62, 63 |
| [Fe(P)(NO)]: BP86/TZVP | 1703 | 595 | 427 | 12.709 | 3.619 | 0.415 | 62, 63 |
| [Fe(P)(NO)]: QCC-NCA | 1698 (1624) | 531 (517) | 371 (365) | 12.530 | 2.975 | 0.336 | 62, 63 |
| [$^{57}$Fe(TPP)(MI)(NO)]: EXP. | 1630 (1556) | 437 (429) | 563 (551) | | | | 62, 63, 64 |
| [Fe(TPP)(MI)(NO)]: BP86/TZVP | 1668 | 606 | 485 | 12.219 | 3.241 | 0.694 | 181 |
| [$^{57}$Fe(TPP)(MI)(NO)]: QCC-NCA | 1630 (1558) | 438 (429) | ~562 (547) | 11.55 | 2.574 | 0.773 | 181 |
| [Fe(P)(MI)(NO)]: BP86/TZVP | 1662 | 609 | 482 | 12.224 | 3.257 | 0.680 | 62, 63 |
| [$^{57}$Fe(P)(MI)(NO)]: QCC-NCA | 1628 (1557) | 439 (427) | 560 (545) | 11.55 | 2.380 | 0.799 | 64 |
| [$^{57}$Fe(TPP)(MI)(NO)][$BF_4$]: EXP. | 1896 (1816) | 578 (~569) | 586 (~575) [b] | | | | 182 |
| [Fe(P)(MI)(NO)]$^+$: BP86/TZVP | 1933 | 639 | 606/598 [b] | 15.62 | 4.82 | ~0.46 | 182 |
| [$^{57}$Fe(P)(MI)(NO)]$^+$: QCC-NCA | 1897 (1815) | 580 (566) | 587 (573) [b] | 15.178 | 3.922 | 0.368/0.406 | 182 |

[a] Values in brackets are for the corresponding $^{15}N^{18}O$-labeled complex. [b] For [$^{57}$Fe(TPP)(MI)(NO)][$BF_4$], this refers to the degenerate linear bending mode. [c] The force constant $f_{Fe-N-O}$ is given in mdyn·Å.

**Scheme 4.** Electronic Structure of Ferrous Heme-Nitrosyls: How Is the Unpaired Electron of NO Distributed between $Fe^{II}$ and NO?

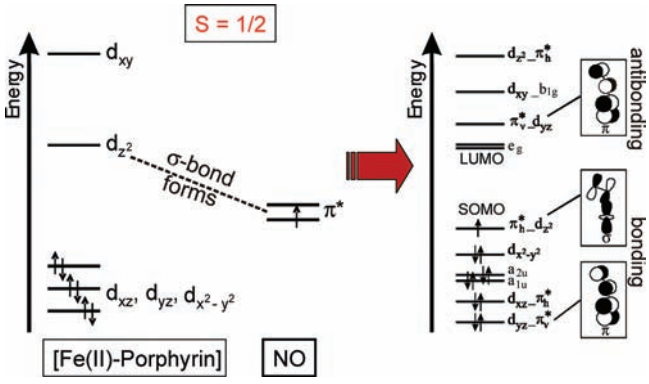


extreme, on the other side, is possible, with the $Fe^{II}$−NO(radical) case being intermediate. Although all of these possibilities fall into the {FeNO}$^7$ regime, they will lead to very different spectroscopic properties and reactivities of the complexes. With the spectroscopic and theoretical methods at hand in the 21st century, we shall therefore aim at going past the Enemark and Feltham classification and achieving more precise descriptions of the electronic structures of transition-metal nitrosyls that reflect the electron distribution in the complexes and the nature of the metal−NO bond, hence allowing one to draw conclusions with respect to the potential reactivities of the complexes. It is one objective of this article to provide the first steps in this direction.

Scheme 4, left, illustrates the central question with respect to the electronic structure of ferrous heme-nitrosyls: *where is the unpaired electron of NO?* As will be shown in the following paragraph, the answer to this question depends on the coordination number (5 or 6) of the complex and the nature of the axial ligand. Scheme 4, right, shows a simplified (restricted open-shell) sketch of the electronic structure of ferrous heme-nitrosyls. Initial theoretical work by Patchkovskii and Ziegler has shown that ferrous heme-nitrosyls show radical character on the bound NO,[163] which was later supported by results from the Oldfield group.[164] On the basis of more detailed, experimentally calibrated electronic structure descriptions presented in refs 62−64, 66, 67, 136, and 159, the spectroscopic properties of these complexes with different types of axial ligands can be understood.

In [Fe(Porphyrin)(NO)] complexes, iron is in the +II oxidation state and low-spin (as evident from EPR), which leads to a [$d_{xz}$, $d_{yz}$, $d_{x^2-y^2}$]$^6$ ≈ [$t_2$]$^6$ electron configuration of the metal, as indicated in Scheme 4, left.[165] NO is a diatomic radical, with one unpaired electron occupying its $\pi^*$ orbitals. Because ferrous heme-nitrosyls exhibit a total spin of $S = {}^1/_2$, the spin-unrestricted scheme has to be applied, which distinguishes between majority (α) and minority ($\beta$) spin orbitals.[166] The unpaired electron of NO occupies the orbital α−$\pi^*_h$ (h = horizontal), which is located in the Fe−N−O plane. Since the $t_2$ orbitals of $Fe^{II}$ are fully occupied, $\sigma$ donation from α−$\pi^*_h$ to the metal is only possible into the $d_{z^2}$ orbital. In the 5C case, the mixing between $\pi^*_h$ and $d_{z^2}$ is very strong, as evident from the corresponding bonding combination $\pi^*_h$_$d_{z^2}$ (the singly occupied molecular orbital, SOMO), which has 23% $\pi^*_h$ and 39% d contribution (plus additional porphyrin orbital admixtures; from BP86/TZVP).[62] Because of mixing with porphyrin orbitals, an additional 18% $d_{z^2}$ occurs in an occupied molecular orbital (MO) at lower energy. In total, this corresponds to a net transfer of about half of an electron from $\pi^*_h$ to $d_{z^2}$ of the $Fe^{II}$ center. Accordingly, the unpaired electron of NO is fully delocalized over the Fe−N−O subunit due to this covalent interaction (cf. Figure 5, left). In agreement with this, calculated spin populations are about +0.5 on iron and +0.5 on NO.[62] Besides this strong Fe−NO $\sigma$ bond, the unoccupied $\pi^*$ orbital of NO, $\pi^*_v$ (vertical), forms

(163) Patchkovskii, S.; Ziegler, T. *Inorg. Chem.* **2000**, *39*, 5354–5364.
(164) Zhang, Y.; Gossman, W.; Oldfield, E. *J. Am. Chem. Soc.* **2003**, *125*, 16387–16396.

(165) In the applied coordinate system (cf. Scheme 3), the $d_{x^2-y^2}$ orbital can formally be identified with one of the $t_2$ orbitals, whereas $d_{xy}$ undergoes a $\sigma$ bond with the porphyrin and can therefore be classified as an e orbital.
(166) Open-shell transition-metal complexes have to be treated in a spin-unrestricted scheme, where the orbitals occupied by the majority (usually α) and minority ($\beta$) spin electrons can differ (spin polarization). For a rigorous analysis, both the α- and $\beta$-MO diagrams therefore need to be considered. Corresponding molecular orbitals are labeled accordingly as, for example, α-$\pi_h$* and $\beta$-$\pi_h$*. In the case of $S = {}^1/_2$ systems as considered here, spin-polarization effects are usually small.

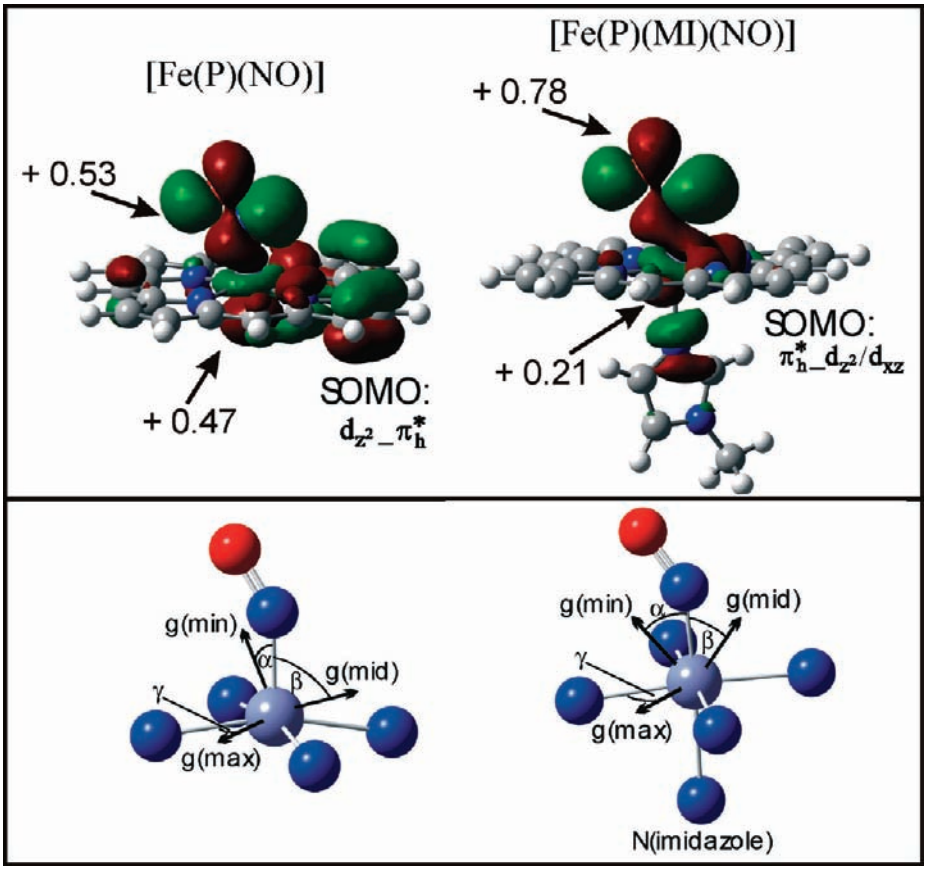


**Figure 5.** Top: Contour plots of the SOMOs of [Fe(P)(NO)] and [Fe(P)(MI)(NO)] calculated with B3LYP/LanL2DZ*. Calculated for the fully optimized structures obtained with BP86/TZVP. The calculated spin densities reflect the shape of the SOMO in both cases. Spin densities on Fe and NO are indicated. Bottom: Calculated orientation of the principal axes of the *g* tensor relative to the molecular frame. Reprinted with permission from ref 63. Copyright 2006 American Chemical Society.

a medium-strong $\pi$ backbond with a fully occupied $d_\pi$ orbital ($d_{yz}$ in Scheme 4) of the $Fe^{II}$ center. The strength of this interaction is estimated best from the corresponding antibonding combination, $\pi^*_v$_$d_{yz}$, which has about 25% metal d character.[62] In a spin-unrestricted scheme, an additional $\pi$ backbond results from the interaction of the (unoccupied) $\beta-\pi^*_h$ orbital with $d_{xz}$. *In summary, NO acts as a strong σ donor and medium-strong π-acceptor ligand in 5C ferrous heme-nitrosyls. Because of the strong σ donation of NO, these complexes have noticeable* $Fe^I-NO^+$ *character.* On the basis of this electronic structure description, trends in the properties of different 5C ferrous heme-nitrosyls can be understood.

**Modulation of $\pi$ Backbonding.** As shown by Spiro and co-workers, the strength of the $\pi$ backbond can be systematically varied in 5C ferrous heme-nitrosyls by adding electron-withdrawing or -donating groups to the phenyl substituents of $TPP^{2-}$-type ligands.[167] This leads to the typical inverse correlation of Fe−NO and N−O bond strengths and corresponding stretching frequencies, where, for example, a strengthening of the $\pi$ backbond (by introduction of an electron-donating substituent) leads to a *stronger* Fe−NO bond and a *higher* $\nu$(Fe−NO) frequency. This goes along with a larger occupation of the $\pi^*$ orbitals of NO involved in the $\pi$ backbond and, in this way (because $\pi^*$ orbitals are N−O antibonding), leads to a *weaker* N−O bond and *lower* $\nu$(N−O) frequency. In this way, Spiro and co-workers were able to modulate the N−O/Fe−NO stretching frequencies between 1663/530 $cm^{-1}$ for the most electron-donating substituent and 1703/514 $cm^{-1}$ for the most electron-withdrawing substituent.[167] The most likely explanation for this finding is that the electron-withdrawing and -donating phenyl substituents modulate the energy of the occupied porphyrin $\pi$ orbitals of $e_g$ symmetry, which interact with the $d_\pi$ orbitals of $Fe^{II}$, responsible for the $\pi$ backbond.[159] For example, electron-donating phenyl substituents likely increase the energy of these porphyrin $e_g$ ($\pi$) orbitals, which, in turn, "push" the $d_\pi$ ($d_{xz}$ and $d_{yz}$) orbitals of $Fe^{II}$ to higher energy and, in this way, closer in energy to the $\pi^*$-acceptor orbitals of NO. In this way, the $\pi$ backbond is strengthened, which increases the Fe−NO bond strength.

**B.2. Binding of Imidazole and Other N-Donor Ligands to Ferrous Heme-Nitrosyls: Weak Ligands with Strong Electronic Effects.**

**Geometric and Spectroscopic Properties.** Scheme 2, right, shows the general structural motif of 6C ferrous heme-nitrosyls [Fe(Porphyrin)(N-donor)(NO)] with axial N-donor coordination *trans* to NO (see Table 3 for structural information), which is very similar to the observed geometries of 5C compounds (Scheme 2, left). Based on this comparison, one could conclude that there is likely not a large difference in the electronic structure between 5C and

(167) Vogel, K. M.; Kozlowski, P. M.; Zgierski, M. Z.; Spiro, T. G. *J. Am. Chem. Soc.* **1999**, *121*, 9915–9921.

6C ferrous heme-nitrosyls and, hence, the coordination number of the corresponding intermediate in the catalytic mechanism of NorBC (cf. Figure 1B), for example, is likely of minor importance. This is further substantiated by the long Fe−(N-donor) bond lengths of ∼2.18 Å as listed in Table 3, indicating that the N-donor is only weakly attached to the iron center and, therefore, should only have a small effect on the electronic structure. This is also in agreement with the small binding constants $K_{eq}$ of proximal N-donor ligands *trans* to NO, which are generally in the range of 1−50 $M^{-1}$.[63,168−170] Correspondingly, a large excess of the N-donor ligand is generally required to generate the 6C complex. The consequences of this issue for the modeling of NorBC are discussed in Section B.5.

The expectation that the weakly coordinated N-donor ligands only have a minor effect on the properties of ferrous heme-nitrosyls is in contrast to spectroscopic findings. From EPR measurements, as shown in Figure 3, it has been known for a long time that binding of an N-donor ligand *trans* to NO has a profound effect on the Fe−N−O unit.[171] Typical *g* values for 6C complexes are about 2.08, 2.00, and 1.98 (cf. ref 66 for details) and, hence, are markedly smaller than those for their 5C analogues. This can be explained based on results from magnetic circular dichroism (MCD) spectroscopy. MCD on 5C and 6C model complexes [Fe(TPP)(NO)] and [Fe(TPP)(MI)(NO)] indicates a distinct decrease of the spin density on iron in the 6C case, as is evident from the appearance of strong diamagnetic MCD signals for the 6C complex.[62] This decrease in the spin density on $Fe^{II}$ generally reduces spin−orbit coupling matrix elements and, in this way, leads to the observed decrease in the *g* shifts.[163] In addition, EPR data of the 6C complexes exhibit the well-resolved hyperfine lines of $^{14}N$ of NO on the medium *g* value, $g_{mid}$, as indicated in Figure 3, right, whereas the well-resolved hyperfine lines in the 5C case are observed on $g_{min}$. Note that the three-line hyperfine pattern of $^{14}N(O)$ is further split by interaction with the $^{14}N$ of the proximal N-donor ligand in the 6C case, generating the nine-line hyperfine pattern evident from Figure 3, right.[172] This distinct difference in the appearance of the EPR spectra of the 5C and 6C complexes is due to a rotation of the *g* tensor in the 6C case, as evident from single-crystal EPR data on Mb−NO and Hb−NO[173,174] and DFT calculations (*vide infra*).[62,63,163] In the 6C complexes, the principal axis of $g_{mid}$ is closest to the Fe−NO axis, whereas in the 5C case, the principal axis of $g_{min}$ is aligned with the Fe−NO vector (cf. Figure 5, bottom). Hence, *the hyperfine lines are well resolved only for the g value whose axis is aligned closest with the Fe−NO bond.*

**Table 3.** Geometric and Vibrational Properties of Selected 6C [Fe(Porphyrin)(L)(NO)]$^{n-}$ (L = N-Donor Ligand or Thiolate; *n* = 0, 1) Complexes in Model Systems and Proteins (See refs 80, 143, 145, and 206 for Additional Examples)

| | geometric parameters [Å][b] | | | | | | vibrational frequencies [cm$^{-1}$] | | | | |
|---|---|---|---|---|---|---|---|---|---|---|---|
| molecule[a] | Δ Fe−N | Δ N−O | ∠Fe −N−O | Δ Fe−$N_P$ | Δ Fe−$L_{tr}$ | ref | ν(N−O) | ν(Fe−NO) | $\delta_{ip}$ (Fe−N−O) | ref | condition |
| $[Fe^{II}(TPP)(MI)(NO)]$ | 1.750 | 1.182 | 138 | 2.008 | 2.173 | 61 | 1630 | 437[c] | 563[c] | 62, 64 | KBr (N−O), solid |
| $[Fe^{II}(TPP)(MI)(^{15}N^{18}O)]$ | | | | | | | 1556 | 429[c] | 551[c] | 62, 64 | |
| $[Fe^{II}(To\text{-}F_2PP)(MI)(NO)]$ | 1.752 | 1.202 | 138 | 2.012 | 2.188 | 63 | 1624 | | | 63 | KBr |
| $[Fe^{II}(TPP)(Me_2NPy)(NO)]$ | 1.758 | 1.170 | 140 | 2.006 | 2.278 | 61 | 1653 | | | 61 | KBr |
| $[Fe^{II}(PPDME)(MI)(NO)]$ | | | | | | | 1618 | | | 209 | MI |
| $Mb^{II}$−NO | 2.03 | 1.14 | 147 | | 2.11 | 194 | 1613 | 443 | 547 | 180, 211 | buffer |
| | 1.89 | 1.15 | 112 | | 2.18 | 193 | | | | | |
| $Hb^{II}$−NO | 1.74 | 1.1 | 145 | | na | 208 | 1615 | | 553 | 212−214 | buffer |
| bovine heart $CCO^{II}$−NO | | | | | | | 1610 | | | 215 | buffer |
| $P450cam^{II}$−NO | | | | | | | 1591 | | 554 | 188, 216, 217 | buffer |
| $[Fe^{II}(TPP)(MI)(NO)]$ (calcd: BP86/TZVP) | 1.741 | 1.186 | 140 | 2.018 | 2.204 | 181 | 1661 | 606[d] | 485[d] | 181 | |
| $[Fe^{II}(TPP)(MI)(NO)]$ (calcd: B3LYP/TZVP) | 1.790 | 1.165 | 140 | 2.024 | 2.156 | 181 | 1787 | 416[e] | 550[e] | 181 | |
| $[Fe^{II}(P)(MI)(NO)]$ (calcd: BP86/TZVP) | 1.734 | 1.186 | 140 | 2.022 | 2.179 | 62 | 1662 | 609[d] | 482[d] | 62 | |
| $[Fe^{II}(P)(MI)(NO)]$ (calcd: B3LYP/LanL2DZ*) | 1.780 | 1.172 | 140 | 2.032 | 2.138 | 181 | 1824 | 417[e] | 539[e] | 181 | |
| $[Fe(P)(SMe)(NO)]^-$ (calcd: BP86/TZVP) | 1.788 | 1.198 | 138 | 2.020 | 2.416 | 67 | 1599 | 440[f] | 531[f] | 67 | |
| $[Fe(P)(SPh)(NO)]^-$ (calcd: BP86/TZVP) | 1.766 | 1.194 | 139 | 2.021 | 2.513 | 67 | 1617 | 569[f] | 465[f] | 67 | |

[a] PPDME = protoporphyrin IX dimethylester$^{2-}$; P = Porphine$^{2-}$ ligand used for calculations. [b] The values for ΔFe−$N_P$ [Fe−N(porphyrin) distance] are averaged; ΔFe−$L_{tr}$ = bond distance between iron and the axial (proximal) ligand *trans* to NO. [c] Determined from NRVS using $^{57}Fe$. Compared to natural abundance isotopes (n.a.i) Fe, the modes ν(Fe−NO) and $\delta_{ip}$(Fe−N−O) appear about 1−2 cm$^{-1}$ shifted to lower energy. [d] From the potential energy distribution (PED) matrix, the mode at ∼610 cm$^{-1}$ has 50−60% Fe−NO stretching and 20−30% Fe−N−O bending contributions. The mode at 485 cm$^{-1}$ is equally mixed. [e] From the PED, the mode at ∼420 cm$^{-1}$ has 30−40% Fe−NO stretching character, but only ∼2% Fe−N−O bending contribution. The feature at ∼550 cm$^{-1}$ has ∼30% Fe−N−O bending and ∼20% Fe−NO stretching character. [f] The Fe−NO stretching and Fe−N−O bending coordinates are equally mixed in the calculation.

(168) Bohle, D. S.; Hung, C.-H. *J. Am. Chem. Soc.* **1995**, *117*, 9584–9585.
(169) Choi, I.-K.; Ryan, M. D. *Inorg. Chim. Acta* **1988**, *153*, 25–30.
(170) Liu, Y.; DeSilva, C.; Ryan, M. D. *Inorg. Chim. Acta* **1997**, *258*, 247–255.
(171) Wayland, B. B.; Olson, L. W. *J. Am. Chem. Soc.* **1974**, *96*, 6037–6041.
(172) Henry, Y. A. Utilization of Nitric Oxide as a Paramagnetic Probe of the Molecular Oxygen Binding Site of Metalloenzymes. In *Nitric Oxide Research from Chemistry to Biology: EPR Spectroscopy of Nitrosylated Compounds*; Henry, Y. A., Guissani, A., Ducastel, B., Eds.; Landes Company: Austin, TX, 1997.
(173) Hori, H.; Ikeda-Saito, M.; Yonetani, T. *J. Biol. Chem.* **1981**, *256*, 7849–7855.
(174) Utterback, S. G.; Doetschman, D. C.; Szumowski, J.; Rizos, A. K. *J. Chem. Phys.* **1983**, *78*, 5874–5880.

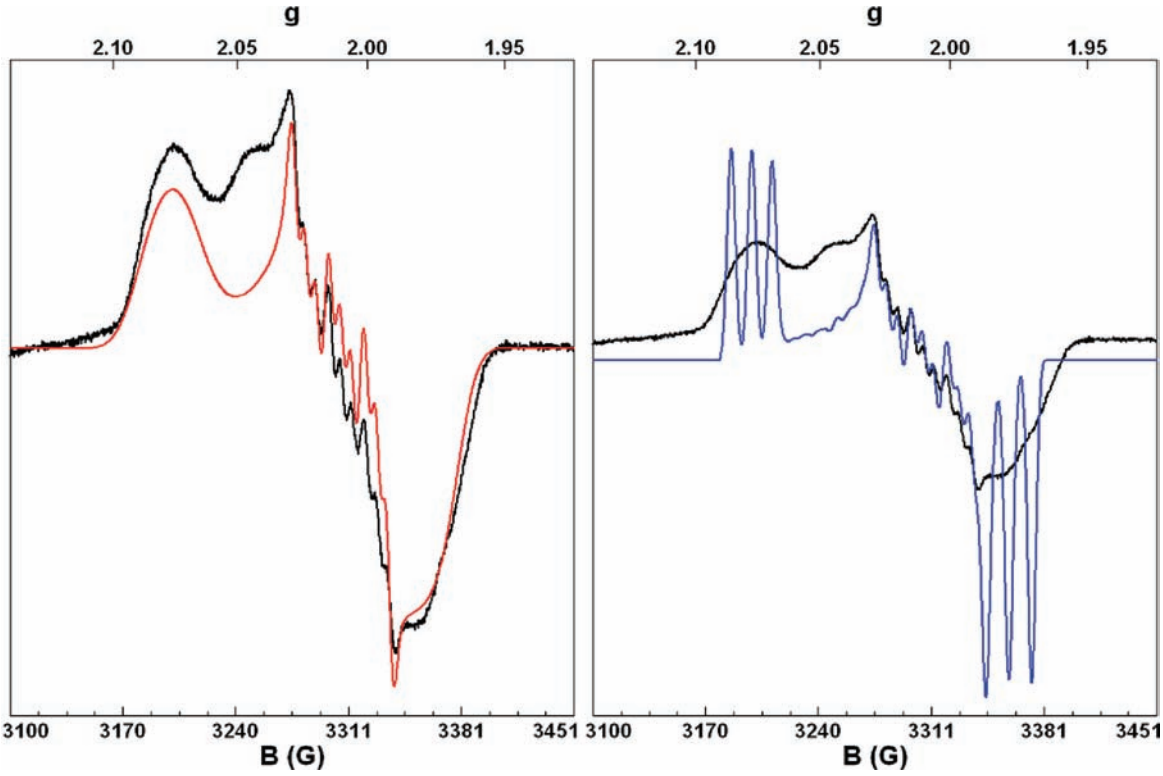


**Figure 6.** EPR spectrum of [Fe(T*o*-$F_2$PP-BzIM)(NO)] in frozen dimethyl sulfoxide at 77 K (black). Left (red): Fit of the spectrum using the program *SpinCount*. Fit parameters: $g_x = 2.077$, $g_y = 2.009$, $g_z = 1.978$. $^{14}$N hyperfine: $^{NO}A_x = 37$ MHz, $^{NO}A_y = 62$ MHz, $^{NO}A_z = 39$ MHz; $^{IM}A_y = 19$ MHz. *g* strain: $\Delta g_x = 0.008$, $\Delta g_y = 0.001$, $\Delta g_z = 0.006$. Right (blue): Fit with the same parameters but with the following *g* strain: $\Delta g_x = \Delta g_y = \Delta g_z = 0.001$.

Because all three components $A_x$, $A_y$, and $A_z$ of the $^{14}$N hyperfine tensor are clearly nonzero for both 5C and 6C ferrous heme-nitrosyls, we believe that this difference is actually due to the well-known disorder of the NO ligand in these compounds: here, the bound NO ligand rotates around the Fe−NO bond,[175,176] leading to different conformations of the complex that are almost isoenergetic.[159,163] This changes the orientation of the principal axes of the *g* values located in the porphyrin plane and, hence, induces slight variations in their magnitudes (the "*g* strain"), whereas the orientation of the axial *g* value remains almost invariant. Because of this disorder, *the g strain for the in-plane g values is larger, which washes out the hyperfine splittings*. This is demonstrated in Figure 6: the fit of the EPR spectrum of the 6C model complex [Fe(T*o*-$F_2$PP-BzIM)(NO)] is shown in red on the left.[65] If the *g* strain in $g_{max}$ and $g_{min}$ is reduced to the much smaller value of $g_{mid}$, the blue spectrum on the right is obtained, where hyperfine lines are now clearly resolved for all three *g* values. Hence, the change in the *g* tensor orientation, combined with the disorder of NO, is responsible for the different appearances of the EPR spectra of the 5C and 6C complexes.

**Vibrational Spectroscopy.** Whereas the vibrational assignments for 5C ferrous heme-nitrosyls are well established as described above, there has been a long-standing controversy about the energies of the Fe−NO stretch $\nu$(Fe−NO) and the Fe−N−O bend $\delta_{ip}$(Fe−N−O) in the 6C case.[177−179] The Fe−NO stretch in $Mb^{II}$−NO was initially assigned to a band at ~550 $cm^{-1}$, and corresponding features have been observed via resonance Raman for 6C ferrous heme-nitrosyls in other proteins. NRVS and resonance Raman spectroscopy on $Mb^{II}$−NO later identified $\nu$(Fe−NO) at 443 $cm^{-1}$ and $\delta_{ip}$(Fe−N−O) at 547 $cm^{-1}$,[180] in agreement with Benko and Yu's initial (re)assignment of the ~550 $cm^{-1}$ feature in $Mb^{II}$−NO and $Hb^{II}$−NO to the Fe−N−O bending mode.[178] In parallel work, we assigned these modes in the 6C model complex [Fe(TPP)(MI)(NO)] using IR, resonance Raman, and NRVS measurements combined with $^{15}N^{18}O$ isotope labeling and QCC-NCA simulations of our data.[62−64,181] Two isotope-sensitive features at 437 and 563 $cm^{-1}$ were identified from NRVS (cf. Figure 4, bottom). To assign these bands, the vibrational energies and isotope shifts of these features were simulated using our QCC-NCA approach. Accounting for the strong out-of-plane polarization of the 437 $cm^{-1}$ feature from single-crystal NRVS measurements,[180,181] $\nu$(Fe−NO) was unambiguously assigned to the band at 437 $cm^{-1}$, and $\delta_{ip}$(Fe−N−O) was identified with the feature at 563 $cm^{-1}$.[64] In this way, NRVS measurements have resolved a long-standing controversy in the literature about the assignment of $\nu$(Fe−NO) in 6C ferrous heme-nitrosyls in proteins and model complexes.

(175) Silvernail, N. J.; Barabanschikov, A.; Sage, J. T.; Noll, B. C.; Scheidt, W. R. *J. Am. Chem. Soc.* **2009**, *131*, 2131–2140.
(176) Silvernail, N. J.; Pavlik, J. W.; Noll, B. C.; Schulz, C. E.; Scheidt, W. R. *Inorg. Chem.* **2008**, *47*, 912–920.
(177) Tsubaki, M.; Yu, N. T. *Biochemistry* **1982**, *21*, 1140–1144.
(178) Benko, B.; Yu, N. T. *Proc. Natl. Acad. Sci. U.S.A.* **1983**, *80*, 7042–7046.
(179) Tomita, T.; Hirota, S.; Ogura, T.; Olson, J. S.; Kitagawa, T. *J. Phys. Chem. B* **1999**, *103*, 7044–7054.
(180) Zeng, W.; Silvernail, N. J.; Wharton, D. C.; Georgiev, G. Y.; Leu, B. M.; Scheidt, W. R.; Zhao, J.; Sturhahn, W.; Alp, E. E.; Sage, J. T. *J. Am. Chem. Soc.* **2005**, *125*, 11200–11201.

The simulation of the vibrational energies for $\nu$(N−O), $\nu$(Fe−NO), and $\delta_{ip}$(Fe−N−O) using our QCC-NCA approach and the porphine approximation described above delivered N−O and Fe−NO force constants of 11.55 and 2.38 mdyn/Å, which were later improved by including the phenyl substituents of $TPP^{2-}$ in the QCC-NCA fit. This led to N−O and Fe−NO force constants of 11.55 and 2.57 mdyn/Å, as shown in Table 2.[181]

In contrast to these assignments, it was recently suggested, on the basis of resonance Raman spectroscopy, that $\nu$(Fe−NO) in [Fe(TPP)(MI)(NO)] is located at 582 $cm^{-1}$, and no feature around 440 $cm^{-1}$ was observed.[156] However, our powder and single-crystal NRVS data of this complex, as described above, clearly show that this 582 $cm^{-1}$ Raman band cannot correspond to the Fe−NO stretch because this mode is, in fact, located at ∼440 $cm^{-1}$. More likely, the 582 $cm^{-1}$ Raman band from ref 156 belongs to $\delta_{ip}$(Fe−N−O), and one could propose that the 19 $cm^{-1}$ difference in frequency compared to our NRVS data might be due to the different conditions applied for the measurements (the NRVS data of [$^{57}$Fe(TPP)(MI)(NO)] are taken on microcrystalline solids, whereas ref 156 presents solution Raman data). However, the N−O stretching frequency seems quite unresponsive to this change in conditions: $\nu$(N−O) is observed at 1623 $cm^{-1}$ in solution[156] and at 1630 $cm^{-1}$ in a KBr disk and in the pure solid.[64] In addition, recent NRVS measurements on [$^{57}$Fe(TPP)(MI)(NO)] in tetrahydrofuran solution do not show any shift in $\delta_{ip}$(Fe−N−O).[181] Alternatively, the 582 $cm^{-1}$ Raman band observed in ref 156 could belong to an impurity of the corresponding ferric complex. It is striking that the vibrational energy of 582 $cm^{-1}$ is very similar to $\nu$(Fe−NO) of the ferric complex [Fe(TPP)(MI)(NO)]($BF_4$), observed at 580 $cm^{-1}$ via NRVS.[182] Further work is necessary to fully understand the puzzling difference between the NRVS and resonance Raman results for 6C ferrous heme-nitrosyl model complexes. Note that this is in contrast to 5C heme-nitrosyls and 6C ferrous heme-carbonyls, where the two techniques deliver comparable vibrational energies.

**Electronic Structure.** The spectroscopic results described above reveal important differences in the electronic structures of 5C and 6C ferrous heme-nitrosyls. Binding of an N-donor ligand *trans* to NO induces a reduction of the spin density on the iron center, as is evident from EPR and MCD spectroscopies[62,66,171] and DFT calculations.[63,163] In addition, both the N−O and Fe−NO bonds are simultaneously weakened, as documented by a shift of $\nu$(N−O) and $\nu$(Fe−NO) from 1670−1700 and 520−540 $cm^{-1}$ in the 5C complexes to 1610−1630 and ∼440 $cm^{-1}$ for the 6C systems (cf. Tables 1 and 3), respectively. Force constants provide an even better measure of the bond strength changes (in closely related complexes) because they are independent of mode mixing.[161] The N−O and Fe−NO force constants for 5C [Fe(TPP)(NO)] of 12.53 and 2.98 mdyn/Å drop to 11.55 and 2.57 mdyn/Å upon binding of MI in the 6C complex [Fe(TPP)(MI)(NO)].[63,64] This *direct correlation* of the N−O and Fe−NO bond strengths indicates a change (weakening) of the Fe−NO $\sigma$ bond upon coordination of the N-donor ligand, whereas a change in $\pi$ backbonding would lead to an inverse correlation (*vide supra*).[63] The weakening of the Fe−NO bond in 6C complexes is further evident from an increase in the NO dissociation constant.[168] $^1$H-NMR spectroscopy has also been used to elucidate the resulting denitrosylation of the complexes.[63]

DFT calculations show that binding of an N-donor ligand in *trans* position to NO reduces mixing of the singly-occupied $\pi^*_h$ orbital of NO with $d_{z^2}$ of $Fe^{II}$ due to a $\sigma$ *trans* interaction with the proximal N-donor ligand[62,63] (see also ref 183 for a qualitative description). In addition, $d_{z^2}$ is rotated off the Fe−NO axis by admixture of $d_{xz}$ character, which further reduces the overlap of $\pi^*_h$ with the resulting $d_{z^2}/d_{xz}$ combination. This weakens the Fe−NO $\sigma$ bond, as reflected by the lower Fe−NO stretching frequency of ∼440 $cm^{-1}$ compared to the 5C case. Because of the reduced donation from the $\pi^*_h$ orbital of NO, the N−O bond is also weakened, as is evident from $\nu$(N−O) observed around 1610−1630 $cm^{-1}$ for the 6C compounds. This explains the experimentally observed direct correlation of the N−O and Fe−NO bond strengths in 5C and 6C heme-nitrosyls as described above (cf. Table 2). This change in the electronic structure is illustrated by the contour plots of the SOMOs of the 5C and 6C complexes in Figure 5. The reduced $\sigma$ donation from NO to $Fe^{II}$ in the 6C case also causes a shift in the spin-density distribution with spin populations of about +0.8 on NO and only +0.2 on iron in 6C complexes, in agreement with the EPR and MCD results.[62,63,66] Earlier DFT calculations found a qualitatively similar trend, but the spin densities are too iron-centered in this case (see Section B.3).[163] On the basis of these descriptions, the 6C complexes correspond to the prototype of an $Fe^{II}$−NO-(radical) adduct, whereas NO is a stronger $\sigma$ donor in the 5C case, giving this complex noticeable $Fe^{I}$−$NO^{+}$ character. On the other hand, the $\pi$ backbond is of comparable strength in analogous 5C and 6C complexes.[62,63] Our DFT calculations also reproduce the rotation of the $g$ tensor in the 6C complexes, as shown in Figure 5, bottom, and, hence, are in agreement with all available experimental data.[62,63]

In conclusion, although N-donor ligands only bind weakly to $Fe^{II}$−NO complexes, they have a measurable effect on the electronic structures of these compounds. This counterintuitive effect is explained by the contour plot of the SOMO of the 6C complexes in Figure 5, right: the interaction of $d_{z^2}$ with the $sp^2$ $\sigma$-donor orbital of MI in the SOMO is actually *antibonding*, directly reflecting the $\sigma$ *trans* interaction/competition between NO and MI for $d_{z^2}$. This weakens the $Fe^{II}$−(N-donor) bond thermodynamically, leading to the experimentally observed small N-donor binding constants, but at the same time allows the N-donor ligand to substantially affect the electronic structure of the $Fe^{II}$−NO unit.

**Modulation of $\sigma$ Bonding.** Because this change of the Fe−NO $\sigma$ bond upon binding of an N-donor ligand is mediated by metal−ligand covalency, the magnitude of this effect depends entirely on the $\sigma$-donor strength of the N-donor ligand. In other words, *the observed weakening of the Fe−NO and N−O bonds in the 6C complexes*

(181) Lehnert, N.; Sage, J. T.; Silvernail, N. J.; Scheidt, W. R.; Alp, E. E.; Sturhahn, W.; Zhao, J., submitted for publication.

(182) Praneeth, V. K. K.; Paulat, F.; Berto, T. C.; DeBeer George, S.; Näther, C.; Sulok, C. D.; Lehnert, N. *J. Am. Chem. Soc.* **2008**, *130*, 15288–15303.

(183) Enemark, J. H.; Feltham, R. D. *J. Am. Chem. Soc.* **1974**, *96*, 5002.

*correlates with the σ-donor strength of the bound N-donor*: the stronger this ligand binds to the $Fe^{II}$ center, the more pronounced is the reduction of the Fe−NO and N−O bond strengths. For example, in [Fe(TPP)(NO)], the N−O stretching frequency is observed at 1697 $cm^{-1}$, which drops to 1630 $cm^{-1}$ upon coordination of the strong N-donor ligand MI, whereas coordination of the weaker 4-(dimethylamino)pyridine ligand ($Me_2NPy$) only reduces $\nu$(N−O) to an intermediate position of 1653 $cm^{-1}$.[61] In this respect, the N−O stretching frequency serves as a direct and very sensitive probe for the donor strength of the proximal N-donor ligand, as documented first by Scheidt and co-workers.[184] In addition, the magnitude of the $^{14}N$ hyperfine coupling constant of the proximal N-donor ligand available from EPR measurements is also a (more indirect) measure of the $Fe^{II}$−(N-donor) bond strength.[65] This is due to the fact that the covalency of the $Fe^{II}$−(N-donor) bond directly correlates with the amount of spin density transferred from the $Fe^{II}$−NO unit to the N-donor atom of the ligand,[63,163] which then correlates with the contact shift and, hence, the magnitude of the $^{14}N$ hyperfine coupling constant of the proximal N-donor ligand.[65]

**Correlation of the N−O Stretch and the Fe−N−O Bend?** 6C ferrous heme-nitrosyls exhibit a Raman band at ∼550 $cm^{-1}$, assigned to $\delta_{ip}$(Fe−N−O), which has been proposed to show an inverse correlation with $\nu$(N−O) in different heme protein NO adducts.[156] Scheme 5 shows a corresponding correlation plot between $\nu$(N−O) and $\delta_{ip}$(Fe−N−O) that includes a number of proteins as well as wild-type (wt) Mb and corresponding active site mutants. These data indicate a quite limited correlation of these vibrational frequencies, which, overall, could be characterized as slightly inverse. On the other hand, if only wt Mb and distal His64 mutants are considered (green data points), the correlation becomes direct.[156] When other Mb mutants are added to the picture, the situation again becomes less defined. Therefore, it is fair to say that the overall correlation between $\delta_{ip}$(Fe−N−O) and $\nu$(N−O) is limited. A recent single-crystal NRVS study on [Fe(TPP)(MI)(NO)] that includes a QCC-NCA fit of the *complete* NRVS spectrum of this compound (cf. Figure 7) provides more insight into this observation. Although the principal assignments of the 437 and 563 $cm^{-1}$ features to $\nu$(Fe−NO) and $\delta_{ip}$(Fe−N−O) do not change,[181] these results show that the Fe−N−O bending internal coordinate is distributed over a number of porphyrin-based vibrations in the 520−580 $cm^{-1}$ region because of strong mode mixing, and the main feature assigned to $\delta_{ip}$(Fe−N−O) is observed at 563 $cm^{-1}$ (cf. Figure 4, bottom). These modes also show quite strong admixtures of the Fe−NO stretching internal coordinate, as evidenced by their out-of-plane polarized intensity as shown in Figure 7, inset. A similar situation is likely encountered in other 6C ferrous heme-nitrosyls, based on the similarities of the vibrational energies. Thus, *the complex and strongly mixed nature of* $\delta_{ip}$*(Fe−N−O) explains the observed lack of correlation with* $\nu$*(N−O)*. In contrast, the Fe−NO stretch appears as a much cleaner mode at ∼440 $cm^{-1}$ and shows only a small admixture of the Fe−N−O bending coordinate.[181]

(184) Scheidt, W. R.; Brinegar, A. C.; Ferro, E. B.; Kirner, J. F. *J. Am. Chem. Soc.* **1977**, *99*, 7315–7322.

**Scheme 5.** Correlation Diagram for $\nu$(N−O) and $\delta_{ip}$(Fe−N−O) in 6C Ferrous Heme-Nitrosyls in Proteins and Model Systems, Using Data from refs 156, 179, and 196. Data for wt $Mb^{II}$−NO and [Fe(TPP)(MI)(NO)] are taken from refs 64 and 180[a]

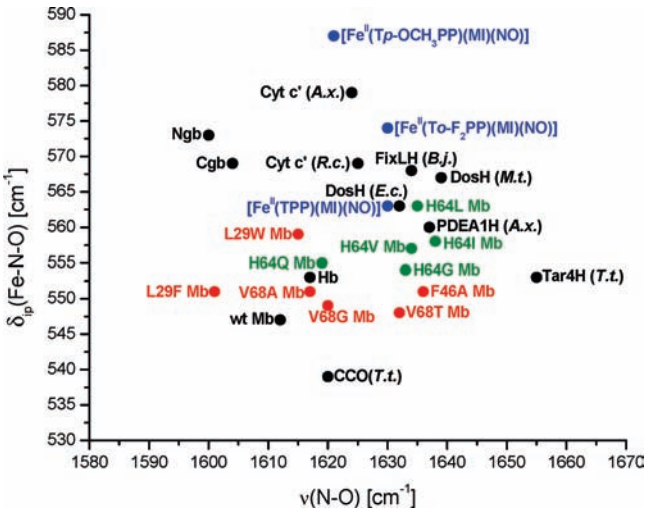


[a] Black: heme proteins with proximal His coordination. Blue: model complexes with bound 1-methylimidazole (MI). Red: Mb mutants. Green: Mb mutants where the distal His64 has been altered to remove the potential hydrogen bond to the coordinated NO.

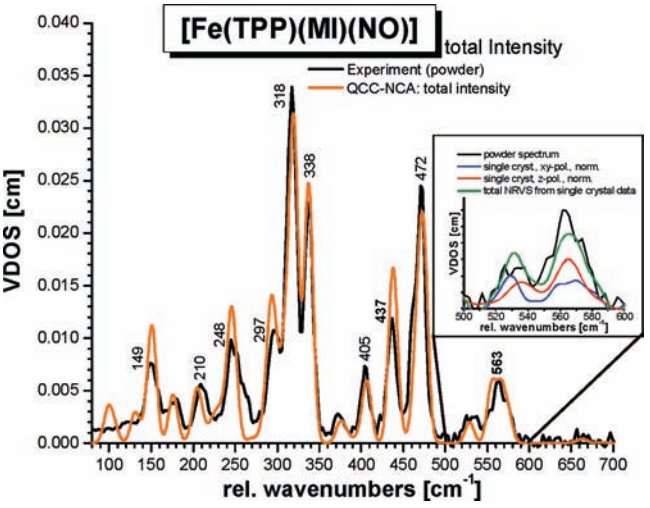


**Figure 7.** Experimental powder data (black) of [$^{57}$Fe(TPP)(MI)(NO)] and total NRVS VDOS intensity from a simulation using the QCC-NCA approach (orange). Inset: NRVS VDOS spectra in the 500−600 $cm^{-1}$ range. Black: powder spectrum. Blue and red: normalized single-crystal in-plane (blue) and out-of-plane (red) polarized spectra. Green: predicted powder spectrum from the single-crystal data. Adapted from ref 181.

**B.3. Ferrous Heme-Nitrosyls: a Challenge for DFT Calculations.** DFT calculations are generally able to reproduce the geometries and vibrational frequencies of the [M(Porphyrin)] core of metalloporphyrin complexes [M(Porphyrin)(L)(L′)] well, as has been demonstrated in the literature.[161,185,186] On the other hand, the properties of the axial L−M−L′ subunit are more of a challenge. This is particularly true for heme-nitrosyls because of the "noninnocence" of this ligand, the presence of an unpaired

(185) Rush, T. S., III; Kozlowski, P. M.; Piffat, C. A.; Kumble, R.; Zgierski, M. Z.; Spiro, T. G. *J. Phys. Chem. B* **2000**, *104*, 5020–5034.
(186) Paulat, F.; Praneeth, V. K. K.; Näther, C.; Lehnert, N. *Inorg. Chem.* **2006**, *45*, 2835–2856.

electron, and the fact that NO also undergoes significant backbonding interactions. Gradient-corrected functionals like BP86, BLYP, or PW91 generally overestimate metal−ligand covalencies and, hence, predict too strong metal−ligand bonds. This is particularly true for the $Fe^{II}$−NO bond in both 5C and 6C ferrous complexes, where both of the Fe−NO $\sigma$ and $\pi$ bond strengths are overestimated. Correspondingly, as shown in Tables 1 and 3, BP86 calculations generally predict too short Fe−NO bonds and Fe−NO stretching frequencies around 600 $cm^{-1}$, compared to experimental values of 520−540 $cm^{-1}$ (5C) and ∼440 $cm^{-1}$ (6C), respectively. The same trend is evident from the Fe−NO force constants, which are overestimated by 0.6−0.8 mdyn/Å compared to the QCC-NCA results (cf. Table 2).

In the case of the N−O bond strength and vibrational frequency, the situation is more complicated (and less insightful) because an overestimation of the Fe−NO $\sigma$ bond (donation *from* an N−O antibonding $\pi^*$ orbital) would result in a too strong N−O bond and, hence, a too high N−O stretching frequency, whereas an overestimation of the Fe−NO $\pi$ backbond (donation *into* an N−O antibonding $\pi^*$ orbital) would lead to a too weak N−O bond and, correspondingly, a too low N−O frequency. Gradient-corrected functionals like BP86 are able to find a good balance between these interactions, leading to predicted $\nu$(N−O) values of 1700−1720 $cm^{-1}$ (5C) and 1660−1680 $cm^{-1}$ (6C), as shown in Tables 1 and 3, which are in good agreement with experiment.

In the case of the hybrid functional B3LYP, the covalency of the Fe−NO $\pi$ backbond is underestimated and, correspondingly, the balance of Fe−NO $\sigma$ and $\pi$ bonding is disturbed. This leads to calculated N−O stretching frequencies of about ∼1800 $cm^{-1}$ in both the 5C and 6C complexes (cf. Tables 1 and 3), which is a substantial error. On the other hand, the calculated Fe−NO bond lengths and stretching frequencies from B3LYP are better compared to BP86 in the 5C case, as evident from Table 1. This indicates that B3LYP is able to generally reduce the Fe−NO covalency, leading to a better result for the description of the Fe−NO bond. A similar improvement is also observed for the 6C complexes, but the competition between $\pi^*_h$ of NO and the $\sigma$-donor orbital of the proximal N-donor ligand for $d_{z^2}$ of iron adds additional complexity in this case. In fact, the balance between the Fe−NO and Fe−(N-donor) bond strengths is not described well with B3LYP either. A comparison of the calculated and experimental Fe−NO force constants for [Fe(TPP)(MI)(NO)] shows that the reality lies, in fact, between the BP86 and B3LYP results:

$$f_{Fe-NO}: \quad \text{BP86 (3.24)} > \text{QCC-NCA (2.57)} > \text{B3LYP (2.18)} \quad \text{[in mdyn/Å]}$$

where BP86 gives a too strong and B3LYP a too weak Fe−NO bond. In the case of the $Fe-N_{IM}$ bond, the trend is roughly inverse:

$$f_{Fe-N(IM)}: \quad \text{B3LYP (0.72)} \approx \text{QCC-NCA (0.78)} > \text{BP86 (0.56)} \quad \text{[in mdyn/Å]}$$

Therefore, QCC-NCA simulations are absolutely crucial to determining reliable force constants, normal-mode

**Table 4.** Geometric and Vibrational Properties of [Fe(Porphyrin)(L)(NO)]$^{n+}$ Complexes (L = N-Donor or Thiolate, or Missing; $n$ = 0, 1). See refs 80, 143, 145, and 182 for Additional Examples

| | geometric parameters [Å][b] | | | | | | vibrational frequencies [$cm^{-1}$] | | | |
|---|---|---|---|---|---|---|---|---|---|---|
| molecule[a] | ΔFe−N | ΔN−O | ∠Fe−N−O | ΔFe−$L_{tr}$ | ΔFe−$N_P$ | ref | $\nu$(N−O) | $\nu$(Fe−NO) | δ(Fe−N−O) | ref |
| [Fe(OEP)(NO)][$ClO_4$][c] | 1.644 | 1.112 | 177 | | 1.994 | 218 | 1868 | 611 | | 219 |
| [Fe(OEP)(MI)(NO)][$ClO_4$] | 1.646 | 1.135 | 177 | 1.988 | 2.003 | 220 | 1921 | | | 220 |
| [Fe(OEP)(Py)(NO)]Cl | | | | | | | | 602 | | 221 |
| [Fe(SP-14)(Py)(NO)]Cl | | | | | | | | 603 | | 221 |
| [Fe(TPP)(NO)][$BF_4$] | | | | | | | 1853 | | | 182 |
| [Fe(TPP)(MI)(NO)][$BF_4$] | | | | | | | 1896 | 580[d] | 587[d]/588 (IR) | 182 |
| [Fe(TPP)(MI)($^{15}N^{18}O$)][$BF_4$] | | | | | | | 1816 | (∼569)[d] | (∼575)[d]/572 (IR) | 182 |
| [Fe(TPP)(NO)($NO_2$)][e] | 1.671 | 1.144 | 169 | 1.998 | 1.996 | 222 | 1874 | | | 182 |
| $Hb^{III}$−NO | | | | | | | 1925 | 594 | | 178, 214, 223 |
| $Mb^{III}$−NO | | | | | | | 1927 | 595 | 572 | 178, 179, 211, 224 |
| $HRP^{III}$−NO | | | | | | | 1903 | 604 | 574 | 178, 209, 224 |
| $P450nor^{III}$−NO | | | | | | | 1851 | 530 | | 132 |
| $P450cam^{III}$−NO | | | | | | | 1806 | 528 | | 132, 225 |
| [Fe(OEP)(SR-$H_2$)(NO)] | 1.671 | 1.187 | 160 | 2.356 | 2.01 | 139 | 1850 | 549[f] | | 139[f] |
| [Fe(P)(MI)(NO)]$^+$ (calcd: BP86/TZVP {$Fe^{II}$−$NO^+$}) | 1.644 | 1.147 | 180 | 2.018 | 2.022 | 182 | 1933 | 639 | 606/598 | 182 |
| [Fe(P)(SR-$H_2$)(NO)] (calcd: BP86/TZVP) | 1.668 | 1.158 | 167 | 2.434 | 2.024 | 204 | 1859 | 604 | 552/539 | 204 |
| [Fe(P)(SPh)(NO)] (calcd: BP86/TZVP) | 1.685 | 1.162 | 164 | 2.343 | 2.027 | 204 | 1829 | 584 | 560/535 | 204 |

[a] MI = 1-methylimidazole; P = $Porphine^{2-}$ ligand used for calculations; HRP = horseradish peroxidase; SP-14 = strapped porphyrin with a 14 atom tether. [b] The values for ΔFe−$N_P$ [Fe−N(porphyrin) distance] are averaged. ΔFe−$L_{tr}$ = bond distance between iron and the axial (proximal) ligand *trans* to NO. [c] Chloroform solvate. [d] From NRVS, natural abundance isotope energies at 580 and 587 $cm^{-1}$ are estimated from the calculated $^{57}$Fe shifts from NCA (experimental NRVS energies: 578 and 586 $cm^{-1}$, respectively). The energies in the $^{15}N^{18}O$ case can only be estimated because only one band is observed spectroscopically centered at 571 $cm^{-1}$. [e] Structural data for [Fe(TpivPP)(NO)($NO_2$)]. [f] This work.

**Table 5.** Calculated (BP86/TZVP) Geometric and Vibrational Properties of $[Fe(P)(L)(NO)]^{n-}$ Complexes (L = MI or $SMe^-$; n = 1,2) and of Corresponding Protonated Species Compared to Experiment

| | geometric parameters [Å][b] | | | | vibrational frequencies [$cm^{-1}$] | | |
|---|---|---|---|---|---|---|---|
| molecule [a] | ΔFe−N | ΔN−O | ∠Fe−N−O | ΔFe−$L_{tr}$ | ν(N−O) | ν(Fe−NO) | ref |
| $[Fe(TPP)(NO)]^-$ | | | | | 1496 | 549 | 226 |
| $[Fe(T\textit{per}\text{-}F_5PPBr_8)(NO)]^-$ | | | | | 1550 | | 227 |
| Mb−HNO | 1.82 | 1.24 | 131 | 2.09 | 1385 | 651 | 200 |
| P450nor: intermediate I | | | | | | 596 | 134 |
| $[Fe(P)(SMe)(NHO)]^-$ (**3a**, $S = 0$) | 1.824 | 1.252 | 133 | 2.354 | 1386 | 601/430 | 136 |
| $[Fe(P)(SMe)(NOH)]^-$ (**3b**, $S = 0$) | 1.746 | 1.401 | 117 | 2.411 | 833 | 649 | 136 |
| [Fe(P)(SMe)(NHOH)] (**4**, $S = 0$) | 1.810 | 1.397 | 125 | 2.230 | 952 | 609/544 [c] | 136 |
| [Fe(P)(MI)(NHO)] ($S = 0$) | 1.789 | 1.236 | 132 | 2.082 | 1459 | 651/464 | [d] |

[a] MI = 1-methylimidazole; P = $Porphine^{2-}$; [b] ΔFe−$L_{tr}$ = bond distance between iron and the axial (proximal) ligand *trans* to NO. [c] Both modes at 609 and 544 $cm^{-1}$ are strongly mixed with in-plane and out-of-plane Fe−N−H bends. [d] This work.

descriptions, and vibrational assignments for ferrous heme-nitrosyls.

In summary, gradient-corrected functionals like BP86 lead to an overall better description of the bond lengths and vibrational frequencies in ferrous heme-nitrosyls. Spin density and total energy calculations are better performed with B3LYP because gradient-corrected functionals clearly overestimate metal−ligand covalencies and, hence, deliver wrong spin distributions and ligand binding energies in these complexes. The ideal solution is therefore to perform geometry optimizations with BP86, followed by spin density and/or total energy calculations with B3LYP on the BP86 structures, and this strategy has proven successful in the analysis of the spectroscopic properties and electronic structures of heme-nitrosyls in a number of cases.[63,182]

Due to the large size of substituted metalloporphyrins, many researchers have used the porphine ($P^{2-}$; cf. Scheme 1) approximation for the analysis of axial ligand binding to hemes. Tables 1 and 3 contain DFT results for porphine complexes in direct comparison with calculations that include the complete porphyrin ligands. Surprisingly, the calculated properties of the porphine models are very similar to the complete molecules if only the axial Fe−N−O subunits are considered, but at a fraction of the computational cost. This emphasizes that porphine is a good approximation for $OEP^{2-}$ and $TPP^{2-}$ for the investigation of axial ligand properties. This approach is also useful for the screening of functional/basis set combinations for following large-scale computations.

Recently, DFT calculations with gradient-corrected functionals were used to predict trends in the Fe−NO vibrational energies in 6C ferrous heme-nitrosyls, for example, upon porphyrin ring substitution or the formation of hydrogen bonds to the coordinated NO.[187] However, this approach is problematic because gradient-corrected functionals predict that the ~600 $cm^{-1}$ mode of the Fe−N−O subunit (cf. Table 3) used in these comparisons has more dominant Fe−NO stretching character with little contibutions from porphyrin-based vibrations. Experimentally, very different normal-mode descriptions are obtained where the vibration at higher energy (540−560 $cm^{-1}$) has more dominant Fe−N−O bending character and shows strong contributions from porphyrin-based vibrations.[181] Hence, because the predictions derived from these DFT calculations are based on incorrect vibrational energies and normal-mode descriptions, the conclusions drawn from these calculations have to be treated with some skepticism. Better insight is, in fact, available from the analysis of the structural changes,[187] as further discussed in Section B.5.

**B.4. The Effect of Thiolate Coordination on Ferrous Heme-Nitrosyls.** In contrast to the wealth of information available for 6C ferrous heme-nitrosyls with axial N-donor coordination, data on corresponding thiolate-bound species are rare. Kincaid et al. showed that the N−O stretch in the ferrous cytochrome $P450_{cam}$ NO adduct is observed at 1591 $cm^{-1}$, which is 25−40 $cm^{-1}$ lower compared to imidazole-bound 6C species. An additional isotope-sensitive feature was observed at 554 $cm^{-1}$ in $P450_{cam}$ (and 542 $cm^{-1}$ in chloroperoxidase).[188,189] These features were originally assigned to the Fe−NO stretch but, in light of the above discussion, likely belong to the Fe−N−O bending mode similar to the 6C complexes with proximal N-donor coordination. This point requires further study. BP86/TZVP calculations on the model system $[Fe(P)(SR)(NO)]^-$ (R = Me, Ph) reproduce the trend in ν(N−O), as shown in Table 3: the predicted N−O stretching frequencies of 1599 (R = Me) and 1617 $cm^{-1}$ (R = Ph) are clearly lower in energy compared to [Fe(P)(MI)(NO)] (1662 $cm^{-1}$; from BP86/TZVP).[67] The calculations also indicate that the thiolate-bound species have weaker Fe−NO bonds; i.e., the calculated Fe−NO force constant drops from 3.26 mdyn/Å in [Fe(P)(MI)(NO)] to 2.38 mdyn/Å in $[Fe(P)(SMe)(NO)]^-$. This indicates a change in σ bonding where thiolate leads to an even stronger σ *trans* interaction (effect) with the bound NO.[67] Correspondingly, the SOMO of $[Fe(P)(SMe)(NO)]^-$ has 41% $\pi^*_h$ and only 24% $d_{z^2}$ contribution, which corresponds to a reduction in the Fe−NO covalency compared to [Fe(P)(MI)(NO)] (cf. Scheme 6). However, this is not the whole story. The B3LYP-calculated spin densities for $[Fe(P)(SMe)(NO)]^-$ of > 1.0 on NO and < 0 on Fe are certainly alarming, whereas "normal" values of +0.78 (NO) and +0.21 (Fe) have been obtained for [Fe(P)(MI)(NO)] (cf. Figure 5). In addition, the B3LYP wavefunction for $[Fe(P)(SMe)(NO)]^-$ shows a distinct amount of spin contamination. We therefore performed a Löwdin−Amos−Hall paired orbital (LAH-PO) analysis of the spin-contaminated wavefunction using the approach of

(187) Xu, C.; Spiro, T. G. *J. Biol. Inorg. Chem.* **2008**, *13*, 613–621.

(188) Hu, S.; Kincaid, J. R. *J. Am. Chem. Soc.* **1991**, *113*, 9760–9766.

(189) Hu, S.; Kincaid, J. R. *J. Biol. Chem.* **1993**, *268*, 6189–6193.

**Scheme 6.** Comparison of the SOMOs of Model Complexes [Fe(P)(NO)], [Fe(P)(MI)(NO)], and [Fe(P)(SMe)(NO)]$^-$, Calculated with BP86/TZVP[62,67]

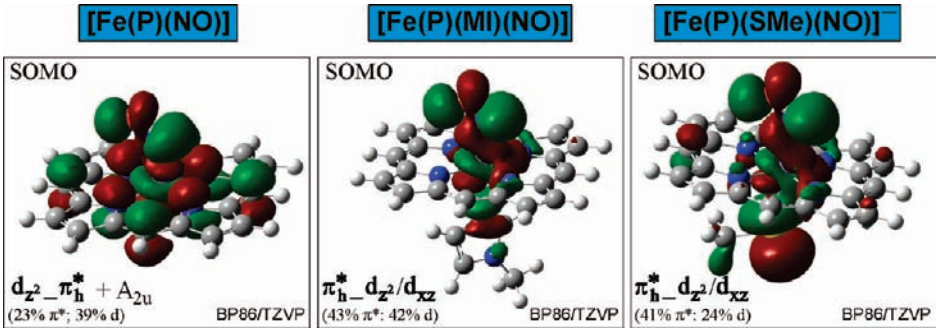


Zilberberg et al.,[190,191] and we found that the observed spin densities reflect the admixture of $Fe^{III}-NO^-$ character into the ground state of $[Fe(P)(SMe)(NO)]^-$. LAH-PO analysis predicts the ground state to have 74% $Fe^{II}-NO$(radical) character with 18% admixture of $Fe^{III}-NO^-$ and 6% contribution from a ligand-field excited state.[136] This originates from the stabilization of $Fe^{III}$ by the anionic thiolate ligand. In contrast, LAH-PO analysis of the B3LYP wavefunction of [Fe(P)(MI)(NO)] delivered a ground state with 88% $Fe^{II}-NO$(radical) character and a 12% admixture of a ligand-field excited state,[136] in agreement with the electronic structure description of this complex developed above.

EPR spectra of ferrous heme-nitrosyls with axial thiolate coordination have been reported for the ferrous NO adducts of P450nor, P450cam, and $P450_{LM}$.[131,192] The obtained $g$ values as well as the well-resolved $^{14}N$ hyperfine lines on $g_{mid}$ both closely resemble the properties of 6C ferrous heme-nitrosyls with N-donor ligands (*vide supra*). On the other hand, the addition of thiophenolate or tetrahydrothiophene to solutions of the 5C complex [Fe(TPP)(NO)] led to EPR spectra that more closely resembled the spectrum of the 5C starting material.[67] These findings indicate that the interaction of the thiophenolates and thioethers (cf. also ref 68) with the $Fe^{II}-NO$ center is much weaker compared to N-donor ligands like imidazole and cysteinate in P450 proteins.

**B.5. Implications for NO Binding to Globins, Signaling, and Catalysis.**

**Implications for NO Binding to Globins.** On the basis of the observation that the strong distal hydrogen bond of His64 to dioxygen is crucial for stable $Fe-O_2$ adduct formation in globins, the effect of the distal His on CO and NO binding to ferrous hemes has also gained considerable attention. Crystallographic investigations on ferrous $Mb^{II}-NO$,[193−195] in fact, implicate the presence of a hydrogen bond between the distal His and NO (cf. Scheme 7), but the strength of this interaction, and, correspondingly, its effect on the properties of the coordinated NO, is not clear. Vibrational spectroscopy is a great method to gain further insight into this issue since metal−NO stretching frequencies are very sensitive reporters of changes in the metal−NO bond, as described above. If the distal His64 in wt Mb is mutated to bulky leucine (H64L) or isoleucine (H64I) to remove the hydrogen bond and (potentially) block the distal pocket, a moderate increase of $\nu$(N−O) from 1613 to 1635−1640 $cm^{-1}$ is observed, accompanied by a distinct shift of $\delta_{ip}$(Fe−N−O) from 547 to ∼560 $cm^{-1}$ (cf. Scheme 5, indicated in green),[196] but, unfortunately, the difference in $\nu$(Fe−NO) is not known. Interestingly, the vibrational properties of these His64 mutants, especially His64L, are very close to those of the model complex [Fe(TPP)(MI)(NO)], indicated in blue in Scheme 5. Hence, this compound is a great model for $Mb^{II}-NO$ in the absence of hydrogen bonding, i.e., for the H64L and H64I mutants. Assuming that the Fe−NO stretching frequency in the model complex and the His64 mutants is also similar, then the energies of $\nu$(Fe−NO) at 443 $cm^{-1}$ in wt $Mb^{II}-NO$ and at ∼439 $cm^{-1}$ (437 $cm^{-1}$ with $^{57}Fe$) in the model complex do not indicate significant changes in the electronic structure because of the presence of the hydrogen bond. Hence, the hydrogen bond is likely relatively weak in the NO case. DFT calculations estimate the hydrogen bond to 3−4 kcal/mol.[197]

In comparison, the lower $\nu$(N−O) frequency in wt Mb−NO might then be due to a simple polarization of the $\pi/\pi^*$

**Scheme 7.** Proposed Hydrogen Bond for NO Bound to Ferrous Globins (See, for Example, refs 41 and 205)

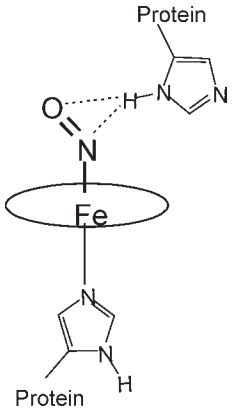


(190) Zilberberg, I.; Ruzankin, S. P. *Chem. Phys. Lett.* **2004**, *394*, 165–170.
(191) Zilberberg, I.; Ruzankin, S. P.; Malykhin, S.; Zhidomirov, G. M. *Chem. Phys. Lett.* **2004**, *394*, 392–396.
(192) O'Keeffe, D. H.; Ebel, R. E.; Peterson, J. A. *J. Biol. Chem.* **1978**, *253*, 3509–3516.
(193) Brucker, E. A.; Olson, J. S.; Ikeda-Saito, M.; Phillips, G. N., Jr. *Proteins: Struct., Funct., Genet.* **1998**, *30*, 352.
(194) Copeland, D. M.; West, A. H.; Richter-Addo, G. B. *Proteins: Struct., Funct., Genet.* **2003**, *53*, 182.
(195) Copeland, D. M.; Soares, A. S.; West, A. H.; Richter-Addo, G. B. *J. Inorg. Biochem.* **2006**, *100*, 1413–1425.
(196) Coyle, C. M.; Vogel, K. M.; Rush, T. S.; Kozlowski, P. M.; Williams, R.; Spiro, T. G.; Dou, Y.; Ikeda-Saito, M.; Olson, J. S.; Zgierski, M. Z. *Biochemistry* **2003**, *42*, 4896–4903.
(197) Tangen, E.; Svadberg, A.; Ghosh, A. *Inorg. Chem.* **2005**, *44*, 7802–7805.

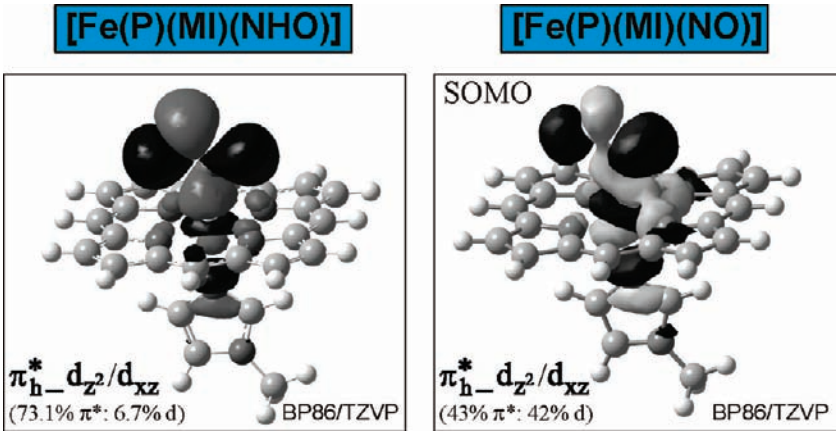


**Figure 8.** *Trans* effect of NO and HNO in 6C ferrous heme complexes: HOMO and SOMO of the model systems [Fe(P)(MI)(NHO)] (left) and [Fe(P)(MI)(NO)] (right), calculated with BP86/TZVP.

orbitals of NO by the hydrogen bond with His64.[181] The larger deviation in vibrational energies observed for the Fe−N−O bend, obtained at 547 $cm^{-1}$ in Mb−NO and at ~560 $cm^{-1}$ in the His mutants and the model complex, might either be due to the sensitivity of this mode to changes in porphyrin vibrations (see Section B.2) or the fact that the polarization of the NO $\pi/\pi^*$ orbitals by the hydrogen bond makes the Fe−N−O subunit less stiff and "easier" to bend. The relatively weak hydrogen bond with His64 in Mb−NO is in agreement with the bonding description of ferrous heme-nitrosyls developed above, where NO binds as a neutral NO(radical) ligand. In contrast, coordination of $O_2$ leads to the formation of an $Fe^{III}-O_2^-$ complex, where the negatively charged superoxide ligand then undergoes a much stronger hydrogen bond with the distal His.[198]

Recently, DFT calculations have been used to obtain further insight into the effect of hydrogen bonding of a distal His on the coordinated NO.[187,197] The results show that different hydrogen bonding geometries are possible that all lead to a slight weakening of the N−O bond in agreement with experiment, whereas in the case of the Fe−NO bond, the effect (strengthening or weakening) depends on the mode of hydrogen bonding. Scheme 5 seems to indicate a weakening of the Fe−NO bond in the hydrogen-bonded case, but one has to keep in mind that the reporter frequency used here at around 550 $cm^{-1}$ actually belongs to the Fe−N−O bend, and, hence, this does not represent conclusive evidence for changes in the Fe−NO bond. On the other hand, the Fe−NO stretch in wt $Mb^{II}$−NO and the model complex [Fe(TPP)-(MI)(NO)] is quite similar (*vide supra*), indicating that the effect of hydrogen bonding on the Fe−NO bond is relatively weak.

**NO Signaling.** In the case of sGC, binding of NO to the ferrous heme active site of this protein leads to the intermediate formation of a 6C complex, followed by transformation of this species into a 5C ferrous heme-nitrosyl due to a breaking of the $Fe^{II}$−His bond.[89] A similar situation is likely encountered in cytochrome *c*′.[70] Whereas it would be quite difficult to measure binding constants of His to the ferrous heme centers in these proteins, this observation can be straightforwardly explained using model complexes. In this case, it has been demonstrated that coordination of NO leads to a substantial weakening of the $Fe^{II}$−imidazole bond, as reflected by the binding constants of imidazole *trans* to NO of only 10−50 $M^{-1}$. This relates to the competition of the $\sigma$-donor orbitals $\pi^*_h$ of NO and Im($\sigma$) for $d_{z^2}$ of iron, which explains the *trans* effect of NO on axially bound N-donor ligands. In the case of the globins, the position of the axial His is restrained, such that stable 6C ferrous heme-nitrosyls are obtained.

It has also been proposed that HNO produced *in vivo* could activate sGC.[199] However, a careful consideration of the model system [Fe(P)(MI)(HNO)] shows that the *trans* effect of HNO is much weaker than that of NO. Figure 8, left, shows the contour plot of the highest occupied molecular orbital (HOMO) of this model system, which has 73% $\pi^*_h$ and only 7% $d_{z^2}/d_{xz}$ character. Although this orbital is antibonding with respect to IM, the contribution of $d_{z^2}$ to this MO is much smaller compared to the SOMO in the corresponding NO model system [Fe(P)(MI)(NO)], which shows 42% $d_{z^2}/d_{xz}$ character (Figure 8, right). The $\sigma$ *trans* effect is therefore much smaller for HNO, and, hence, this molecule is not likely to activate sGC.[89] This trend is further reflected by the optimized $Fe^{II}-N_{MI}$ bond distance in these models, which is 2.179 Å for NO compared to 2.082 Å for the HNO complex (compared to 2.09 Å for Mb-HNO[200]). Finally, the calculated binding constant of MI is about 3−4 orders of magnitude larger for the HNO compared to the NO complex.

**Implications for Catalysis.** As shown in Figure 1B, a ferrous heme-nitrosyl is catalytically active in the formation of $N_2O$ from NO in NorBC, but details of the N−N coupling mechanism are unknown. In addition, it is not clear whether the heme-nitrosyl is 5C or 6C; in light of the above discussion, both coordination numbers seem possible. Our results have demonstrated that the presence of an axial ligand (of N- or S-donor type) *trans* to NO weakens both the Fe−NO and N−O bonds relative to the corresponding 5C species and, in this way, could help to activate NO for catalysis by increasing the amount of

(198) Sigfridsson, E.; Ryde, U. *J. Biol. Inorg. Chem.* **1999**, *4*, 99.

(199) Miranda, K. M. *Coord. Chem. Rev.* **2005**, *249*, 433–455.

(200) Immoos, C. E.; Sulc, F.; Farmer, P. J.; Czarnecki, K.; Bocian, D. F.; Levina, A.; Aitken, J. B.; Armstrong, R. S.; Lay, P. A. *J. Am. Chem. Soc.* **2005**, *127*, 814–815.

**Scheme 8.** Radical versus Dipolar N−N Coupling Mechanism in NorBC[a]

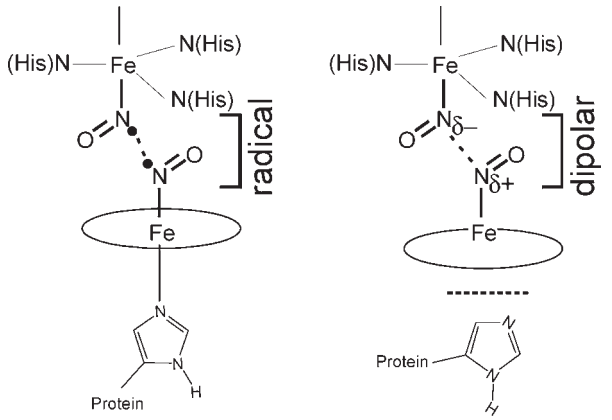


[a] On the basis of the obtained electronic structure descriptions for ferrous heme-nitrosyls (see the text), it can be expected that the 6C complex is more reactive in a radical-type reaction, whereas the 5C complex could potentially be advantageous for a dipolar-type coupling.

radical character (spin density) on the coordinated NO.[63] This finding could be of key importance for the activation of NO in NorBC because ferrous heme-nitrosyls are generally stable and quite unreactive.[92] In the proposed radical-type N−N coupling mechanism in Figure 1B, a 6C ferrous heme-nitrosyl would then be expected to be more reactive due of the increased radical character on the bound NO. On the other hand, the electronic structure of ferrous nonheme-nitrosyl complexes might be best described as $Fe^{III}-NO^{-}$, where the high-spin ferric center ($S = {}^{5}/_{2}$) and the $NO^{-}$ ligand ($S = 1$) are antiferromagnetically coupled to give the $S = {}^{3}/_{2}$ ground state.[201] A similar $Fe_B-NO$ complex with a $S = {}^{3}/_{2}$ ground state has also been observed for NorBC.[101] On this basis, the N−N coupling process might be better described as a dipolar reaction between the nonheme $Fe_B^{III}-NO^{-}$ species and the heme-nitrosyl, which would then be expected to be more reactive in the 5C state that shows noticeable $Fe^{I}-NO^{+}$ character. Scheme 8 shows both possible N−N coupling mechanisms.

Since the coordination number influences the electronic structure and reactivity of the bound NO ligand, further experimental studies on corresponding 5C and 6C model complexes are desirable. These experiments are challenging in the 6C case because the synthesis of a ferrous heme-nitrosyl that is 6C in solution at room temperature in the absence of excess N-donor ligand (which could influence the reactivity studies) is difficult because of the strong $\sigma$ *trans* effect of NO. We recently succeeded in the synthesis of a corresponding model complex (cf. Scheme 9) where the axial imidazole ligand is covalently linked to the porphyrin macrocycle.[65] This result is based on a detailed study of the binding properties of N-donor ligands to 5C ferrous heme-nitrosyls, and it was shown that coordination of the N-donor ligand is facilitated by (a) the choice of IM as the axial ligand, (b) the application of a slightly electron-poor porphyrin derivative, and (c) the usage of a rigid benzyl linker. With these results in hand, further reactivity studies can now be performed.

(201) Brown, C. A.; Pavlosky, M. A.; Westre, T. E.; Zhang, Y.; Hedman, B.; Hodgson, K. O.; Solomon, E. I. *J. Am. Chem. Soc.* **1995**, *117*, 715–732.

**Scheme 9.** Stable 6C Ferrous Heme-Nitrosyl Model Complex in the Absence of Excess Axial Ligand, [Fe(T*o*-$F_2$PP-BzIM)(NO)] (Reprinted with Permission from ref 65. Copyright 2009 American Chemical Society)

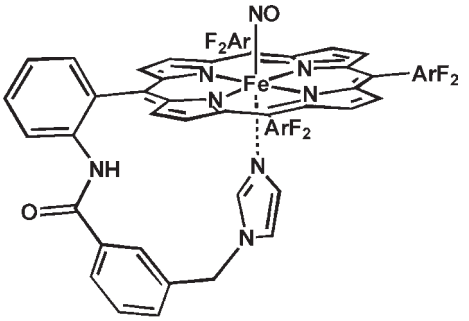


## C. Ferric Heme-Nitrosyls

### C.1. NO as a Weak Ligand That Forms a Strong Metal−Ligand Bond.

**Geometric and Spectroscopic Properties.** Ferric heme-nitrosyls with axial N-donor coordination are characterized by extremely short Fe−NO bond lengths of ∼1.65 Å and linear Fe−N−O units, as listed in Table 4. Vibrational spectroscopic studies of proteins and model complexes show N−O stretching frequencies in the 1900 $cm^{-1}$ region and Fe−NO stretching energies of ∼590 $cm^{-1}$ (cf. Table 4). For example, ferric Mb-NO exhibits $\nu$(N−O) at 1927 $cm^{-1}$ and $\nu$(Fe−NO) at 595 $cm^{-1}$, which compares well to the model complex [Fe(TPP)(MI)(NO)]($BF_4$), where N−O and Fe−NO stretching frequencies of 1896 and 580 $cm^{-1}$ (578 $cm^{-1}$ measured with $^{57}$Fe) have been found.[182] From NCA, force constants of 15.18 mdyn/Å for N−O and 3.92 mdyn/Å for the Fe−NO bond, respectively, have been determined for this model complex, based on IR and NRVS measurements.[182] These geometric and vibrational properties are in agreement with the widely accepted $Fe^{II}-NO^{+}$ description of the electronic structures of ferric heme-nitrosyls.[29] Because the ground states of these compounds are diamagnetic, no additional information is available from EPR or MCD spectroscopies. DFT calculations using gradient-corrected functionals and sufficiently large basis sets are able to reproduce these ground-state properties well (cf. Table 4). As in the ferrous case (see Section B.3), the metal−ligand covalency is overestimated by this method, and, correspondingly, the Fe−NO stretching frequency is predicted somewhat too high in energy, although the deviation from experiment is noticeably smaller here compared to the ferrous case. On the other hand, the N−O frequency is obtained quite close to the experimental value. Again, the porphine approximation works very well if only the properties of the axial Fe−N−O unit are considered.

**Electronic Structure and Comparison to Ferrous Heme-Nitrosyls.** The Fe−NO interaction in the $Fe^{II}-NO^{+}$ ground state of ferric heme-nitrosyls is entirely dominated by strong $\pi$ backbonding between two $d_\pi$ orbitals of the metal ($d_{xz}$ and $d_{yz}$ in the principal coordinate system applied here; cf. Scheme 3) and two empty $\pi^*$ orbitals of $NO^{+}$. Figure 9, left and middle, shows the corresponding antibonding combinations, which have about 70% metal and 30% $\pi^*$ character, corresponding to a very strong interaction. In this respect, $NO^{+}$ is, in fact, a stronger backbonding ligand than CO. The strong $\pi$ backbond leads to a net transfer of the charge density

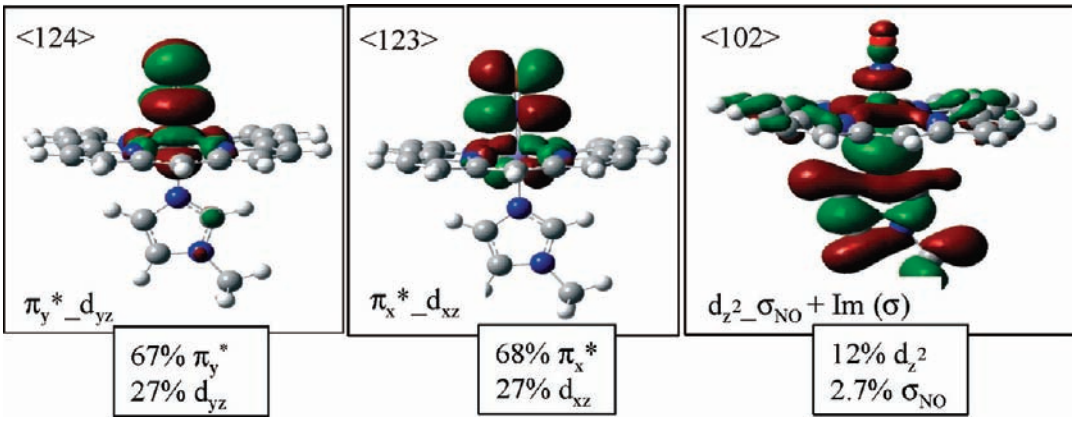


**Figure 9.** Contour plots of key molecular orbitals of ferric heme-nitrosyls in the $Fe^{II}-NO^+$ ground state. Reprinted with permission from ref 182. Copyright 2008 American Chemical Society.

of one electron from the metal to the ligand[202] and explains the lowering of the N−O stretching frequency from 2390 $cm^{-1}$ in free $NO^+$ to ~1900 $cm^{-1}$ in these complexes. In contrast, the Fe−NO $\sigma$ interaction in ferric heme-nitrosyls is weak because of the generally poor donor abilities of the $\sigma_{nb}$ orbital in diatomics with multiple bonds (cf. Figure 9, right). Corresponding to this strong $\pi$ and weak $\sigma$ bonding description, the Fe−N−O unit is linear and short to maximize the $\pi$ interaction.

This quantitative description of the Fe−NO bond in ferric heme-nitrosyls allows for a detailed comparison with the corresponding ferrous complexes described above. The one-electron reduction of ferric heme-nitrosyls is mostly *ligand centered*, in agreement with their $Fe^{II}-NO^+$ electronic structure, resulting in a shift of $\nu$(N−O) from 1896 $cm^{-1}$ in [Fe(TPP)(MI)(NO)]($BF_4$) to 1630 $cm^{-1}$ in [Fe(TPP)(MI)(NO)], for example. The strong Fe−NO $\sigma$ bond in the ferrous complex explains the large thermodynamic stability of the Fe−NO bond in this case and the observed *trans* interaction of the NO ligand with axially coordinated N-donor ligands, which induces long $Fe^{II}-N_{IM}$ bond lengths compared to the corresponding bis(imidazole)-ligated iron(II) porphyrins.[61] In contrast, the $\sigma$ bond is clearly much weaker in ferric heme-nitrosyls, which explains the very short Fe−NO bonds and the lack of a significant *trans* effect of NO in these compounds.[182]

A more rigorous comparison of the Fe−NO bond strength in ferrous and ferric heme-nitrosyls could be based on either thermodynamic or spectroscopic criteria. Experimental complex formation constants $K_{eq}$ of ferrous compared to ferric heme-nitrosyls differ, in general, by 4−5 orders of magnitude. The corresponding NO adduct formation energies $\Delta G^0$ with respect to the reaction, [Fe(Porphyrin)(N-donor)] + NO → [Fe(Porphyrin)-(N-donor)(NO)] are about −15 to −16 kcal/mol for ferrous ($K_{eq}$ = $10^{11}-10^{12}$ $M^{-1}$) versus −4 to −7 kcal/mol ($K_{eq}$ = $10^3-10^5$ $M^{-1}$) for ferric heme-nitrosyls,[203] and this trend is reproduced by DFT total energy calculations.[182] Therefore, *the Fe−NO bond is thermodynamically much stronger in the ferrous compared to the ferric case*. In contrast, a quantitative evaluation of the vibrational data via NCA shows that the Fe−NO force constant is 3.92 mdyn/Å for ferric $[Fe(TPP)(MI)(NO)]^+$ compared to 2.57 mdyn/Å for ferrous [Fe(TPP)(MI)(NO)] (cf. Table 2). *This means that, spectroscopically, the Fe−NO bond is stronger in the ferric compared to the ferrous case, which contradicts the observed thermodynamic trend*. Hence, NO is a weak ligand to ferric heme (from thermodynamics) *but at the same time* makes a strong Fe−NO bond (from spectroscopy)! The basic understanding of NO binding to ferric hemes developed so far is therefore clearly incomplete.

**The Energy Landscape of NO Binding to Ferric Hemes.**[182] To understand the above-described properties of ferric heme-nitrosyls, two key excited states have to be considered. Figure 10 shows the calculated potential energy surfaces (PESs) for (a) the $Fe^{II}-NO^+$ ($S$ = 0, blue) ground state, (b) the open-shell singlet low-spin (ls) $Fe^{III}$−NO(radical) alternative ground state, where ls $Fe^{III}$ is antiferromagnetically coupled to NO ($S$ = 0, red), and (c) the corresponding high-spin (hs) $Fe^{III}$−NO(radical) state ($S$ = 2, black), which corresponds to the product state upon dissociation of NO (because the 5C ferric heme-imidazole complex is high-spin). The PES for the $Fe^{II}-NO^+$ ground state is very steep, with an estimated dissociation energy of > 30 kcal/mol. This is not surprising since the dissociation of the complex into $Fe^{II}$ and $NO^+$ is energetically unfavorable. This explains the spectroscopically observed strength of the Fe−NO bond in ferric heme-nitrosyls: this is, in fact, a property of the $Fe^{II}-NO^+$ ground state of these complexes.

The elusive, alternative ground state ls-$Fe^{III}$−NO-(radical) ($S$ = 0) does, in fact, exist as an energy minimum and is observed surprisingly close in energy to the

(202) This corresponds to an effect of covalency because the electron density transferred to the iron center has the charge of approximately one electron but no spin due to the transfer of equivalent amounts of $\alpha$ and $\beta$ spin density. Hence, this does not correspond to an electron transfer since an electron has a charge and a spin.

(203) It should be noted that the equilibrium constant of NO binding relates to the difference in free energy, $\Delta G°$, between the NO-bound complex and the dissociation products upon NO release. Therefore, the major contribution to $\Delta G°$ comes from the strength of the heme−NO bond. However, as pointed out by Ford and co-workers, a small part of the difference, at least in a coordinating medium such as an aqueous solution, comes from the fact that NO is replaced by a solvent molecule, which contributes to the stability of the product. Indeed, the difference in the mechanism of NO binding between $Fe^{III}$(Porphyrin) and $Fe^{II}$(Porphyrin) complexes in aqueous media can be largely attributed to the role of coordinated solvent in the former case. See: Laverman, L. E.; Hoshino, M.; Ford, P. C. *J. Am. Chem. Soc.* **1997**, *119*, 12663–12665. Laverman, L. E.; Ford, P. C. *J. Am. Chem. Soc.* **2001**, *123*, 11614–11622.

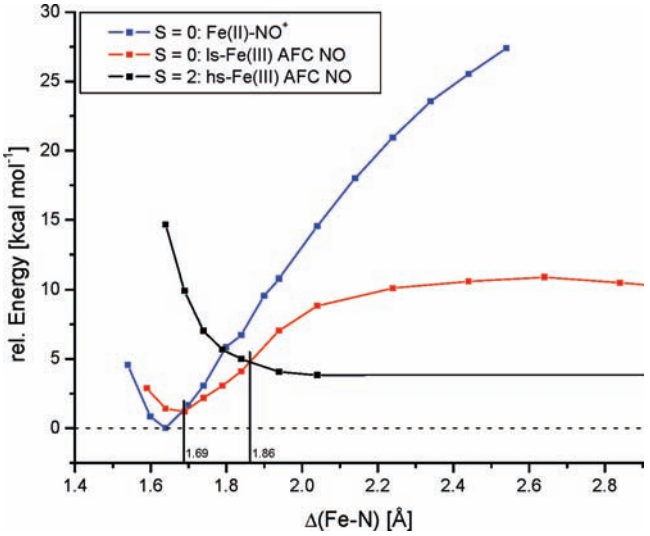


**Figure 10.** Calculated potential energy surfaces (PESs) for 6C ferric heme-nitrosyls using the model system $[Fe(P)(MI)(NO)]^+$ (P = porphine$^{2-}$; MI = 1-methylimidazole). The following states are considered: (a) closed-shell $Fe^{II}-NO^+$ (blue); (b) low-spin (ls) $Fe^{III}$ antiferromagnetically coupled (AFC) to NO (open shell $S = 0$; red); (c) high-spin (hs) $Fe^{III}$ AFC to NO ($S = 2$; black). Reprinted with permission from ref 182. Copyright 2008 American Chemical Society.

$Fe^{II}-NO^+$ ground state (DFT energy separation: only ~1 kcal/mol). However, the calculated energy difference between these states is likely underestimated by a few kilocalories per mole, as is evident from the vibrational properties, which do not indicate the presence of the ls-$Fe^{III}$−NO(radical) state close to the ground state. In addition, the ground state is likely stabilized by configuration interaction (CI) via the corresponding, doubly excited electronic state within the Fe−NO $\pi$ backbond. Taking this into consideration, the energy surfaces of the $Fe^{II}-NO^+$ ground state and the ls-$Fe^{III}$−NO(radical) state cross at an Fe−NO distance of about 1.70−1.76 Å; i.e., the ground state of the complex changes (cf. Figure 10), accompanied by the transfer of one electron from $Fe^{II}$ back to $NO^+$.

Importantly, the properties of the two states, $Fe^{II}-NO^+$ and ls-$Fe^{III}$−NO(radical), are very different, as illustrated in Scheme 10. From the calculations, the ls-$Fe^{III}$−NO(radical) state has a weaker (longer) Fe−NO bond and, hence, a lower Fe−NO stretching frequency. Because of the electron transfer from $Fe^{II}$ into a $\pi^*$ orbital of $NO^+$, the N−O bond is also weaker, giving rise to $\nu$(N−O) at lower frequency. *Compared to experiment, it is therefore apparent that all ferric heme-nitrosyl complexes characterized so far fall into the regime of the $Fe^{II}-NO^+$ ground state*. Upon a further elongation of the Fe−NO bond, the ls-$Fe^{III}$−NO(radical) crosses the hs-$Fe^{III}$−NO(radical) energy surface ($S = 2$) at a Fe−NO distance of ~1.9 Å. This transition corresponds to a spin crossover of $Fe^{III}$ and is related to the fact that the 5C ferric heme product is actually high-spin. Importantly, *the hs-$Fe^{III}$−NO(radical) PES is dissociative with respect to the Fe−NO bond*. This dramatically lowers the thermodynamic stability of the ferric Fe−NO complex, from about −10 kcal/mol on the ls-$Fe^{III}$−NO(radical) surface to only about −4 kcal/mol (calculated) in the hs-$Fe^{III}$−NO(radical) state. Therefore, *the properties of the hs-$Fe^{III}$−NO(radical) energy surface determine the thermodynamic weakness of the Fe−NO bond in ferric heme-nitrosyls and the large dissociation rate constant of NO*. This means that once the system has entered the hs-$Fe^{III}$−NO(radical) electronic state the dissociative nature of this energy surface will actually drive the NO away from the metal center. Hence, the experimentally derived Fe−NO force constant is *not* a measure for the stability of the Fe−NO bond in this case. *These quantities are actually completely unrelated because they depend on the properties of different electronic states*. In this way, NO can form a strong Fe−NO bond and *at the same time* be a weak ligand to ferric hemes.

**Scheme 10.** Electronic Structures of Ferric Heme-Nitrosyls (Reprinted with Permission from ref 182. Copyright 2006 American Chemical Society)

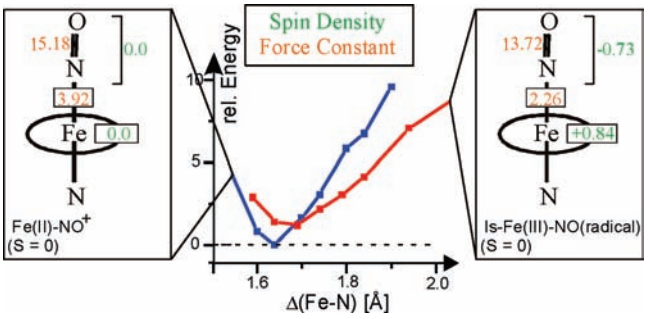


**C.2. The Effect of Thiolate Coordination: a $\sigma$ Backbond into the Fe−N−O $\sigma^*$ Orbital.** The first indication that thiolate coordination to ferric heme-nitrosyls might lead to interesting changes in the properties of these complexes came from the crystal structure of ferric P450nor with bound NO.[127] As shown in Scheme 11, left, this structure exhibits a bent Fe−N−O unit with an Fe−N−O angle of ~160°. This result led to speculations on whether this is due to (a) a steric effect of the protein's active site pocket that would force the Fe−N−O unit to bent or (b) an electronic effect. In 2006, Richter-Addo and co-workers showed that the bent Fe−N−O unit is, in fact, an intrinsic feature of these complexes. As shown in Scheme 11, right, the crystal structure of the complex [Fe(OEP)(SR-$H_2$)(NO)] [SR-$H_2$ = S-2,6-$(CF_3CONH)_2$-$C_6H_3$] shows the same bending of the Fe−N−O unit (angle: 160°),[139] which provides strong evidence that this is due to an electronic effect related to the presence of the thiolate ligand *trans* to NO. Another consequence of thiolate coordination becomes apparent from the vibrational data, as shown in Table 4: N−O and Fe−NO stretching frequencies of about 1820−1850 and 510−530 $cm^{-1}$ are observed, respectively, for ferric heme-nitrosyls with cysteinate coordination, which are distinctively lower in energy compared to the imidazole ligated proteins, where $\nu$(N−O) and $\nu$(Fe−NO) are found at ~1900 and ~590 $cm^{-1}$, respectively. To determine whether this trend also holds for model compounds, we then investigated the complex [Fe(OEP)(SR-$H_2$)(NO)] using resonance Raman spectroscopy. The precursor, [Fe(OEP)(SR-$H_2$)], was reacted with 1 equiv of NO at low temperature, and the formation of the corresponding NO adduct was first monitored using in situ UV−Vis spectroscopy. As shown in Figure 11, upon NO exposure, the Soret band of [Fe(OEP)(SR-$H_2$)] at 380 nm disappears

**Scheme 11.** Ferric Heme-Thiolate NO Complexes: (Left) Crystal Structure of P450nor$^{III}$−NO;[127] (Right) Model Complex, [Fe(OEP)(SR-$H_2$)(NO)][139] (Reprinted with Permission from ref 139. Copyright 2006 Royal Society of Chemistry)

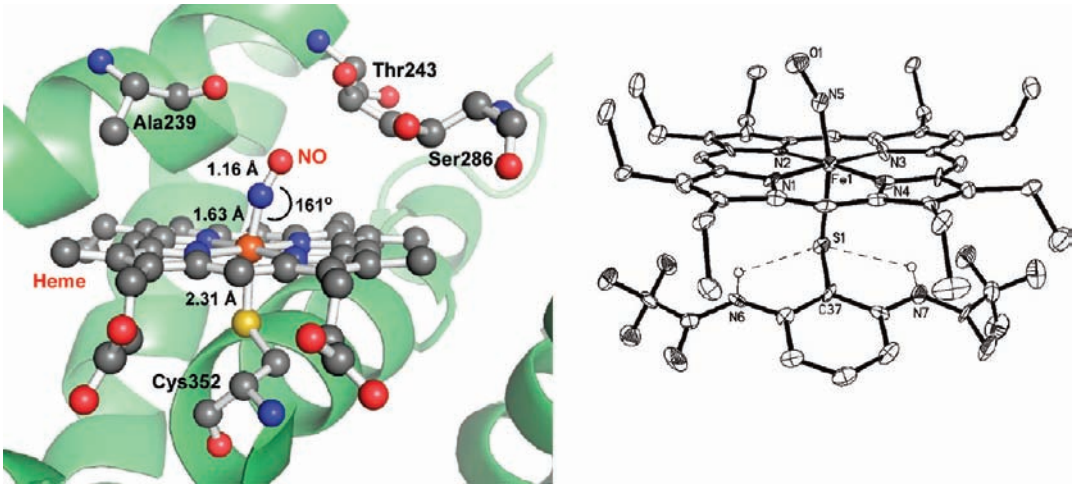


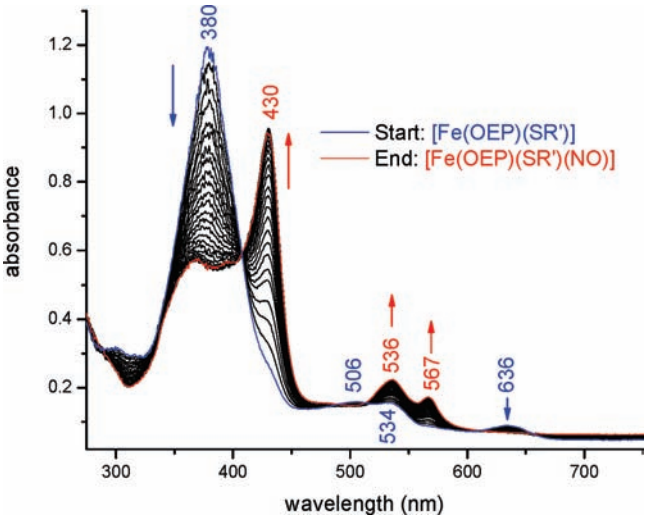


**Figure 11.** UV−Vis titration of the ferric precursor [Fe(OEP)(SR-$H_2$)] (blue) with NO (final spectrum: red).

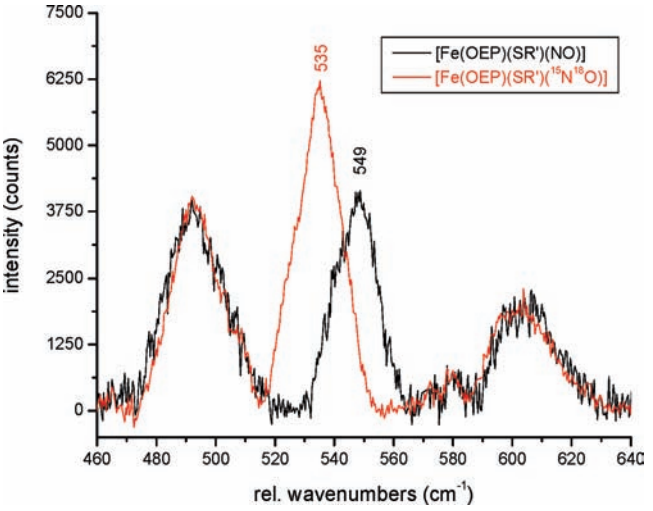


**Figure 12.** Resonance Raman spectra of [Fe(OEP)(SR-$H_2$)(NO)] (black) and of the corresponding $^{15}N^{18}O$-labeled complex (red).

while at the same time new features at 430, 536, and 567 nm grow in, indicative of the formation of [Fe(OEP)(SR-$H_2$)-(NO)]. Raman samples prepared from the reaction mixture show the Fe−NO stretch at 549 cm$^{-1}$, which shifts to 535 cm$^{-1}$ if $^{15}N^{18}O$ is used, as shown in Figure 12. From IR spectroscopy, $\nu$(N−O) of this complex has been observed as a very weak feature (due to decomposition) at ∼1850 cm$^{-1}$.[139] The model complex data therefore support the above conclusion that the coordination of a thiolate ligand *trans* to NO lowers both the N−O and Fe−NO stretching frequency compared to imidazole-bound ferric heme-nitrosyls. This direct correlation of the N−O and Fe−NO frequencies and, hence, bond strengths is indicative of a change in the Fe−NO $\sigma$ bond, whereas a change in the $\pi$ backbond would lead to an inverse correlation (see Section B.1). In summary, the axially coordinated thiolate ligand imposes a $\sigma$ *trans* effect on the coordinated NO, which weakens both the Fe−NO and N−O bonds and induces a bending of the Fe−N−O unit.[204]

This effect was further investigated computationally using a series of model systems [Fe(P)(SR)(NO)], from which, starting from the original ligand SR-$H_2^-$ (Figure 13, left), the hydrogen bonds were stepwise removed.[204] This leads to a stepwise increase of the thiolate donor strength and, hence, the strength of the Fe−S bond as reflected by the Fe−S force constant shown in yellow in Figure 13, which increases along the series: SR-$H_2^-$ < SR-$H_1^-$ < $SR^-$ = $SPh^-$ < $SMe^-$. At the same time, both the Fe−NO (red) and N−O (black) force constants are stepwise reduced, indicative of a $\sigma$ *trans* interaction with thiolate. However, as discussed above, the $\sigma$-donor bond between $\sigma_{nb}$ of NO and $d_{z^2}$ is intrinsically weak, and so it is hard to envision how a change in this interaction could generate these effects. A closer inspection of the MO diagram of the model systems provides, in fact, a different explanation. The anionic thiolate ligand has a $\sigma$-donor orbital at high energy (close to the d manifold), as shown in Figure 14, that mediates the Fe−S $\sigma$ bond. This orbital shows an admixture of an (unoccupied) Fe−N−O $\sigma^*$ orbital that is antibonding with respect to both the Fe−NO and N−O bonds.[204] Hence, partial occupation of this orbital by a

(204) Paulat, F.; Lehnert, N. *Inorg. Chem.* **2007**, *46*, 1547–1549.

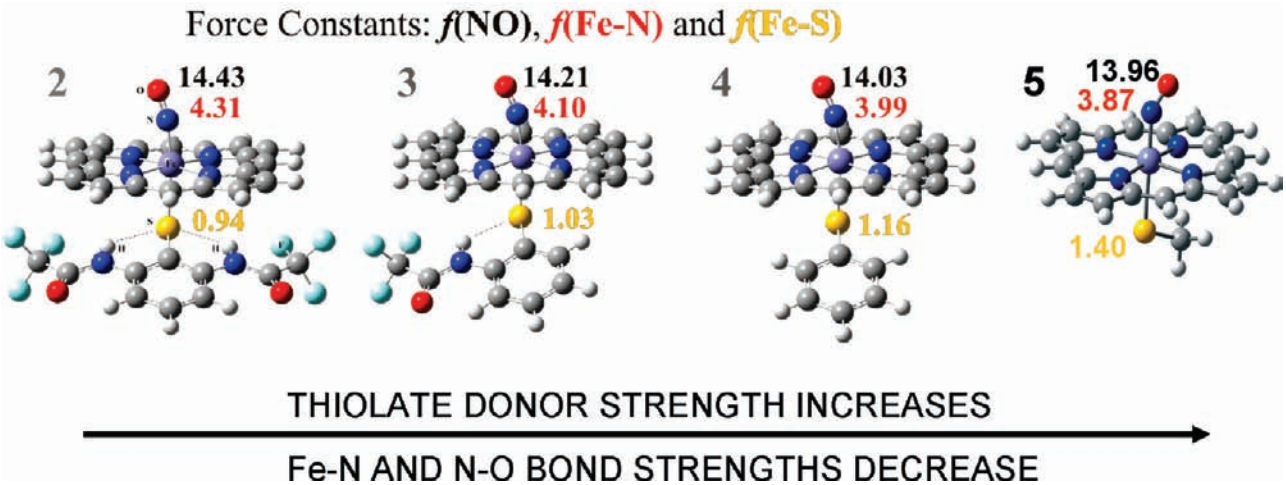


**Figure 13.** Strengthening of the Fe−S bond (Fe−S force constant in yellow) and simultaneous weakening of both the Fe−NO and N−O bonds (force constants in red and black, respectively) in model complexes [Fe(P)(SR)(NO)] along the series SR = SR-$H_2^-$, SR-$H_1^-$, $SPh^-$, and $SMe^-$ giving evidence for a $\sigma$ *trans* effect of the coordinated thiolate on the Fe−N−O moiety in ferric heme-nitrosyls. Calculated with BP86/TZVP.

covalent admixture into the occupied Fe−S $\sigma$-bonding MO *weakens* both the Fe−NO and N−O bonds simultaneously. The correlation of this effect with the strength of the Fe−S bond is due to the fact that a stronger donating thiolate ligand has the Fe−S bonding orbital at even higher energy, which increases mixing with the Fe−N−O $\sigma^*$ orbital. Hence, *the σ trans effect of thiolate on the coordinated NO in ferric heme-nitrosyls is due to the formation of a σ backbond into the σ* orbital of NO*,[204] which is a new type of interaction in heme-nitrosyl chemistry. The partial occupation of the $\sigma^*$ orbital also explains the bending of the Fe−N−O unit in the thiolate-coordinated case, which somewhat reduces the Fe−NO antibonding effect, as illustrated in Figure 14B. However, this bending is only worth about 1 kcal/mol.[204]

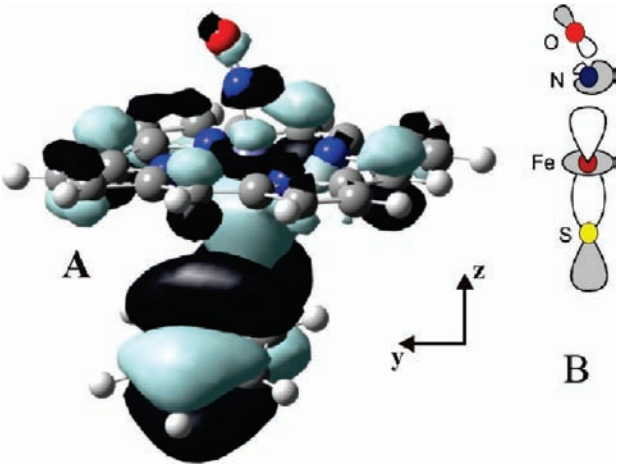


**Figure 14.** Contour plot (left) and schematic drawing (right) of the key molecular orbital $A_{2u} + p_z(S)\_d_{z^2}/d_{xz}\_\sigma^*$ of [Fe(P)(SPh)(NO)], which illustrates the $\sigma$ backbond into the $\sigma^*$ orbital of the Fe−N−O subunit, mediated by the S-donor orbital $p_z$. Reprinted with permission from ref 204. Copyright 2007 American Chemical Society.

**C.3. Implications for NO Transport and Catalysis. NO Transport.** Recently, it was proposed that the ferric heme NO adducts in nitrophorins might have an electronic structure that corresponds to $Fe^{III}$−NO(radical) in order to prevent autoreduction.[76] However, the experimental data available for ferric heme NO adducts with axial N-donor coordination in proteins and model complexes show that these species have the assumed $Fe^{II}-NO^+$ ground state (from Fe−NO bond distances and the Fe−NO and N−O stretching frequencies). For example, the N−O stretching frequency of ferric rNp1−NO of 1917 $cm^{-1}$ is very close to the values

(205) Eich, R. F.; Li, T.; Lemon, D. D.; Doherty, D. H.; Curry, S. R.; Aitken, J. F.; Mathews, A. J.; Johnson, K. A.; Smith, R. D.; Phillips, G. N., Jr.; Olson, J. S. *Biochemistry* **1996**, *35*, 6976–6983.
(206) Wyllie, G. R. A.; Scheidt, W. R. *Inorg. Chem.* **2003**, *42*, 4259–4261.
(207) Silvernail, N. J.; Olmstead, M. M.; Noll, B. C.; Scheidt, W. R. *Inorg. Chem.* **2009**, *48*, 971–977.
(208) Deatherage, J. F.; Moffat, K. *J. Mol. Biol.* **1979**, *134*, 401–417.
(209) Maxwell, J. C.; Caughey, W. S. *Biochemistry* **1976**, *15*, 388–396.
(210) Pal, B.; Kitagawa, T. *J. Inorg. Biochem.* **2005**, *99*, 267–279.
(211) Miller, L. M.; Pedraza, A. J.; Chance, M. R. *Biochemistry* **1997**, *36*, 12199–12207.
(212) Chottard, G.; Mansuy, D. *Biochem. Biophys. Res. Commun.* **1977**, *77*, 1333–1338.
(213) Stong, J. D.; Burke, J. M.; Daly, P.; Wright, P.; Spiro, T. G. *J. Am. Chem. Soc.* **1980**, *102*, 5815–5819.
(214) Wang, Y.; Averill, B. A. *J. Am. Chem. Soc.* **1996**, *118*, 3972–3973.
(215) Zhao, X.-J.; Sampath, V.; Caughey, W. S. *Biochem. Biophys. Res. Commun.* **1994**, *204*, 537–543.
(216) Nagano, S.; Shimada, H.; Tarumi, A.; Hishiki, T.; Kimata-Ariga, Y.; Egawa, T.; Suematsu, M.; Park, S. Y.; Adachi, S.; Shiro, Y.; Ishimura, Y. *Biochemistry* **2003**, *49*, 14507–14514.
(217) Unno, M.; Christian, J. F.; Sjodin, T.; Benson, D. E.; MacDonald, I. D.; Sligar, S. G.; Champion, P. M. *J. Biol. Chem.* **2002**, *277*, 2547–2553.
(218) Ellison, M. K.; Schulz, C. E.; Scheidt, W. R. *Inorg. Chem.* **2000**, *39*, 5102–5110.
(219) Linder, D. P.; Rodgers, K. R.; Banister, J.; Wyllie, G. R. A.; Ellison, M. K.; Scheidt, W. R. *J. Am. Chem. Soc.* **2004**, *126*, 14136–14148.
(220) Ellison, M. K.; Scheidt, W. R. *J. Am. Chem. Soc.* **1999**, *121*, 5210–5219.
(221) Lipscomb, L. A.; Lee, B.-S.; Yu, N.-T. *Inorg. Chem.* **1993**, *32*, 281–286.
(222) Ellison, M. K.; Schulz, C. E.; Scheidt, W. R. *Inorg. Chem.* **1999**, *38*, 100–108.
(223) Sampath, V.; Zhao, J.; Caughey, W. S. *Biochem. Biophys. Res. Commun.* **1994**, *198*, 281–287.
(224) Tomita, T.; Haruta, N.; Aki, M.; Kitagawa, T.; Ikeda-Saito, M. *J. Am. Chem. Soc.* **2001**, *123*, 2666–2667.
(225) Hu, S.; Kincaid, J. R. *J. Am. Chem. Soc.* **1991**, *113*, 2843–2850.
(226) Choi, I.-K.; Liu, Y.; Feng, D.; Paeng, K.-J.; Ryan, M. D. *Inorg. Chem.* **1991**, *30*, 1832–1839.
(227) Pellegrino, J.; Bari, S. E.; Bikiel, D. E.; Doctorovich, F. *J. Am. Chem. Soc.* **2010**, *132*, 989–995.

**Scheme 12.** Calculated Mechanism of P450nor.[136] Free energies given are relative to species **3a**

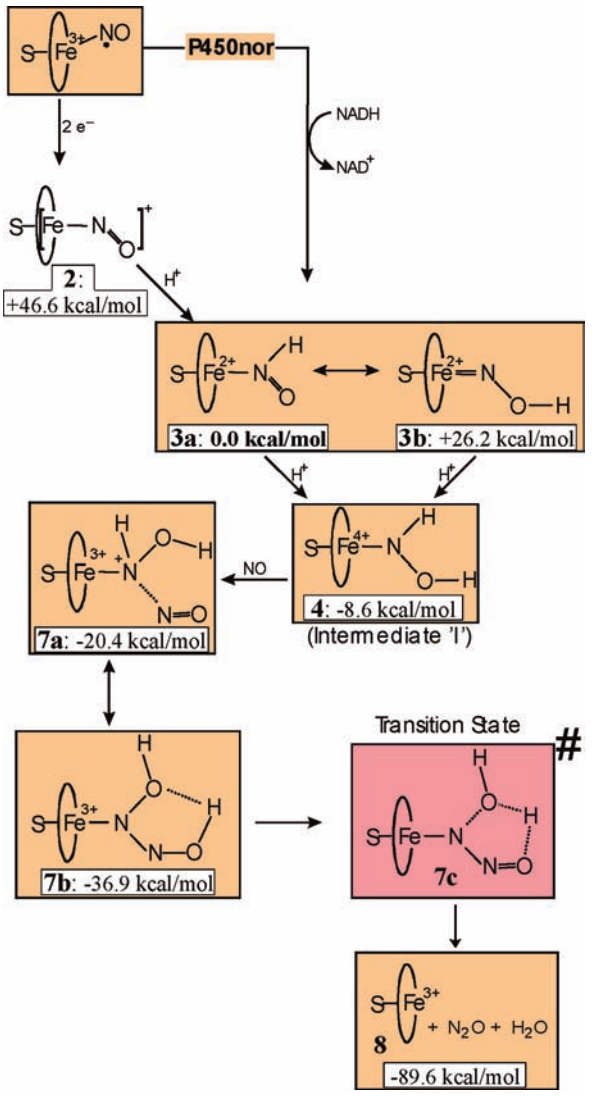


obtained for other ferric proteins and model complexes with axial N-donor coordination (cf. Table 4). Hence, this indicates that the ferric nitrophorin NO adducts do not differ in their electronic structures from the other ferric nitrosyl species.[182] The necessity to use ferric compared to ferrous hemes for NO transport relates to the fact that NO is easily dissociated from ferric hemes as described above. Because the lability of the ferric heme NO bond is an intrinsic feature due to the low energy of the dissociative hs-$Fe^{III}$−NO(radical) state, both proximal His and Cys are suitable ligands for NO transport in nitrophorins.

**The Catalytic Mechanism of P450nor.**[136] Scheme 12 shows the catalytic cycle of P450nor obtained from DFT calculations including relative free energies as indicated. Importantly, the two-electron reduction of the ferric heme-nitrosyl complex (**2**) leads to a formal iron(II)-nitroxyl intermediate that is extremely basic. This means that *the reaction of the iron(III) nitrosyl with NADH has to be considered as a hydride transfer* (see also ref 135) The $Fe^{II}$−NHO complex (**3**) generated is still basic enough to pick up a proton from aqueous solution. The basicity of this species is due to the axial thiolate ligand, which is an attractive explanation for the function of the cysteinate in the active site of P450nor for catalysis. This leads to the generation of a formal $Fe^{IV}$−NHOH intermediate (**4**), which is ideally set up for the reaction with the second molecule of NO. We believe that intermediate I in the original mechanism in Figure 2B corresponds to this NHOH complex. Experimentally, vibrational spectroscopy could be used to determine the protonation state of intermediate I. As shown in Table 5, the singly protonated NHO and NOH tautomers and the doubly protonated NHOH complex show significant differences in their Fe−N and N−O stretching frequencies. Previous experiments identified the Fe−N stretch of intermediate I at 596 $cm^{-1}$,[134] which rules out the NOH tautomer. Identification of the N−O stretch would allow one to distinguish between the NHO and NHOH options. The following reaction of the $Fe^{IV}$−NHOH species with NO can be interpreted as a two-step process, where outer-sphere electron transfer takes place first from the incoming NO to reduce the formal $Fe^{IV}$ center. The generated $NO^+$ then attacks the bound NHOH ligand, resulting in N−N bond formation. After rearrangement, an $Fe^{III}$−$N_2H_2O_2$ ($N_2H_2O_2$ = hyponitrous acid) complex (**7b**) is obtained, which is predicted to be quite stable. Decomposition of this species then produces the products $N_2O$ and water.

## D. Conclusions

In recent years, great progress has been made in the understanding of the electronic structures and reactivities of ferrous and ferric heme-nitrosyls. New results allow one to determine the electron distribution in these complexes and to better classify the bound NO ligands as $NO^+$, NO(radical), or $NO^-$. These electronic structure descriptions are directly related to reactivity as a coordinated $NO^+$ reacts with nucleophiles (base), $NO^-$ is protonated by (weak) acids, and NO(radical) has been proposed to undergo radical reactions with superoxide or another coordinated NO. As new biological roles of $NO_{(x)}$ species emerge, these results will be useful in understanding the reactivities of these species in biological systems.

**Note Added in Proof:** A very recent paper by Olson, Czernuszewicz, Spiro, and co-workers (*J. Am. Chem. Soc.* **2010**, *132*, 4614−4625), shows an inverse correlation of $\nu$(N−O) and $\nu$(Fe−NO) in ferric Mb−NO complexes of wt and mutants. This is in agreement with the idea that the $Fe^{II}$−$NO^+$ ground state of ferric heme-nitrosyls is dominated by $\pi$ backbonding.

**Acknowledgment.** Over the years, this work was supported by the Deutsche Forschungsgemeinschaft (DFG; Grant LE 1393/1-2), the Fonds des Verbandes der Chemischen Industrie (FCI), and currently by the Dow Corning Corp. and a grant from the National Science Foundation (Grant CHE 0846235).

**Supporting Information Available:** Experimental Section including details of the DFT calculations on [Fe(P)(MI)(HNO)], EPR simulations in Figure 6, and spectroscopic measurements on [Fe(OEP)(SR-$H_2$)(NO)]. This material is available free of charge via the Internet at http://pubs.acs.org.